Macromolecules

pubs.acs.org/Macromolecules
Article

A Gram−Charlier Analysis of Scattering to Describe Nonideal Polymer Conformations

Anukta Datta, Xiaoyan Wang, Shawn D. Mengel, Audra J. DeStefano, Rachel A. Segalman, Patrick T. Underhill,* and Matthew E. Helgeson*

Cite This: Macromolecules 2024, 57, 9518−9535

ABSTRACT: Theories of interpreting polymer physics and rheology at the molecular level from experiments, including small-angle scattering, typically rely on the assumption that polymer chains possess a Gaussian configuration distribution. This assumption frequently fails to describe features of real polymer molecules both at equilibrium (when polymers have nonlinear topology or heterogeneous chemistry) and out of equilibrium (when they are subjected to nonlinear deformations). To better describe non-Gaussian polymer conformation distributions, we propose a moments analysis based on the Gram−Charlier expansion as a natural framework for describing structure and scattering from non-Gaussian polymers. The expansion describes the conformation distribution in terms of cumulants (equivalent to moments of the distribution) of the underlying segment density distribution function, providing low-dimensional descriptors that can be inferred directly from measured scattering in a way that is agnostic to a polymer's topology, chemistry, or state of deformation. We use this framework to show that cumulants can be used to "fingerprint" non-Gaussian conformation distributions of polymers either at equilibrium (applied to sequence-defined heteropolymers) or out of equilibrium (applied to polymers experiencing nonlinear deformation due to flow). We anticipate that this new analysis method will provide a general framework for examining nonideal polymer configurations and the properties that arise from them.

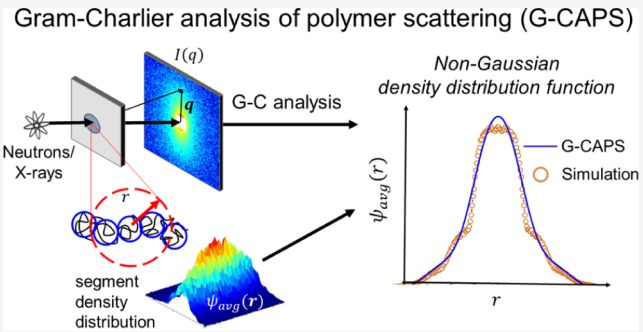

INTRODUCTION

Molecular theories for polymers often rely on the assumption that the configuration of polymer chains behave ideally, according to a Gaussian distribution.[1,2] This includes statistical properties such as the distribution of end-to-end vectors or the distribution of segmental density about the polymer center of mass. Furthermore, the Gaussian chain model is also often used to describe coarse-grain inter- and intramolecular interactions between polymers, as well as effective interactions in binary (polymer−polymer and polymer−solvent) mixtures. As a result, many properties of polymers are theoretically described in terms of Gaussian parameters such as the radius of gyration (for isotropic structures) or equivalently the gyration tensor (for anisotropic structures) or other properties derived from them.

While the assumption of a Gaussian configurational distribution is generally suitable for describing the structure and properties of long-chain homopolymers at or near equilibrium (e.g., under linear deformations), it often proves insufficient in describing the complex nature of real polymer chains, especially in scenarios involving nonlinearity, heterogeneity, and dynamic or out-of-equilibrium processes.[3] Common instances involving such deviations from Gaussian statistics include heteropolymers such as biopolymers,[4] polymers with nonlinear or branched topologies,[5] entangled polymers where correlations between different segments lead to non-Gaussian spatial distributions,[6,7] polymers in confinement or at interfaces,[8,9] glassy or highly cross-linked polymers,[10] and polymers subjected to nonequilibrium conditions such as during deformation or under external forces.[11] The non-Gaussian characteristics of the distribution functions can arise from a number of factors including excluded volume effects,[12,13] nonlinear chain stiffness,[14] and hydrodynamic interactions,[15,16] complex topology-defined internal dynamics,[17] and comonomer-specific interactions.[18] Hence, there is a significant need for a framework to describe non-Gaussian statistics of the configurational distributions that are compatible with both experiments and molecular

Received: May 22, 2024
Revised: August 23, 2024
Accepted: September 23, 2024
Published: October 11, 2024

https://doi.org/10.1021/acs.macromol.4c01169
Macromolecules 2024, 57, 9518−9535

simulation to achieve a comprehensive understanding of their structure−property relationships.

A motivating example of non-Gaussian behavior involves polymer deformations in flow, which strongly influence polymer dynamics, processing, and mechanical properties. Under sufficiently strong hydrodynamic forces, polymer conformations undergo a significant departure from Gaussian behavior, due to both the spectrum of configurational relaxation dynamics and the finite extensibility of chain segments, under highly nonlinear deformations. Understanding and studying the non-Gaussian response of polymers in different flow fields has been a central focus in polymer physics since its early stages.[19,20] For example, in extension-dominated flows, the competition of hydrodynamic forces and nonlinear entropic forces leads to the well-studied coil−stretch transition due to non-Gaussian polymer stretching.[21,22] By contrast, in shear-dominated flows, polymers do not achieve quasi-steady stretching and instead continually experience temporal fluctuations between stretching and tumbling, leading to highly non-Gaussian average distributions in the polymer conformations.[23,24] These phenomena are typically described in simple rheological theories by modeling chains as nonlinear elastic springs[21] with finite extensibility,[25] resulting in predictions of heterogeneous distributions of stretch along a chain.[26] Hur et al.[19] showed that in such cases, the spatial distribution of the polymer segments about its center of mass shifts from a nearly Gaussian shape at low deformation rates to a broad-shaped, skewed distribution at higher deformation rates. Benoit et al.[27] have shown that on extension, the chain ends appear to extend more than the central section indicating a nonuniform stretch distribution across the length of the chain. As a result, the applicability of Gaussian statistics and properties based on them is strongly limited in the limit of large deformations and strain rates, motivating the need for a more general framework to assess non-Gaussian polymer configurations.

In this work, we attempt to take some initial steps toward developing such a framework. We focus particularly on a description of the segment density probability distribution function (subsequently referred to as the segment PDF), which describes the spatial distribution of different polymer segments with respect to the center of mass.[28] For ideal chains at equilibrium, works by Isihara[29] and by Debye and Bueche[30] showed analytically that the PDF under such situations is Gaussian, with variance given by the mean-square radius of gyration $\langle R_g^2 \rangle$ of the polymer chain. Although the density PDF is spherically symmetric at equilibrium, the instantaneous shape of the polymer can be highly anisotropic, and this anisotropy can be described by decomposing R_g^2 into components along its three principal axes for any given chain conformation, referred to as the gyration tensor $G = \langle R_g R_g \rangle$ of the molecule.[31] We chose the segment density distribution as the primary choice for describing non-Gaussian polymer conformations in this work because it can be easily accessed in both molecular simulations and experimental measurements including small-angle scattering.

In principle, spectroscopic measurements such as polarized light birefringence[32] as well as small-angle scattering using various radiation sources (light,[33] X-rays,[34] and neutrons[35]) can be used to characterize intramolecular polymer structure. In these methods, the size and shape of an isolated polymer molecule can be determined by studying the angular dependence of scattered light, as initially described by Peterlin et al.[36] Recently, the advent of single-molecule imaging techniques on DNA using fluorescence microscopy allows for the direct observation of polymer chain configurations and provides unambiguous insights into the principles governing polymer mechanics.[37−40] Similarly, advanced spectroscopic techniques such as double electron−electron resonance (DEER)[41,42] and Förster resonance energy transfer (FRET)[43,44] measure the ensembles of distances between molecular probes, providing full distributions of chain-end conformations. Experimental findings from both bulk and single-molecule structural characterization techniques coupled with molecular simulations have played a pivotal role in developing and predicting the nonequilibrium behavior of polymers.[45] Among these methods, scattering stands out as the most accessible approach to unambiguously examine both the global and local structures of polymer chains, either at equilibrium or under the influence of external forces like flow.[46−49] In particular, there has been growing recent interest in directly correlating the rheological response of a polymer fluid to the internal structure on all relevant length scales, and measurements to probe the spatiotemporal evolution of structure in the nonequilibrium deformed state have been outlined in a recent review by Eberle and Porcar.[50]

The scattered intensity measured in small-angle light, X-ray, or neutron scattering (SALS, SAXS, and SANS) encodes the entire segment density distribution of the polymer. Existing analyses for scattering from polymers either explicitly assume a Gaussian PDF or resort to Fourier-space measures of the scattering function that require a specific real-space structural model to be physically interpreted. For example, the canonical Guinier approximation is used to estimate R_g models, the low-q scattering (where q is the scattering vector) via a Gaussian approximation, but ignores higher-q features of the scattering arising from finer-scale details of the density PDF.[51] Likewise, conventional scattering functions with full q-range support for polymers at equilibrium, such as the Debye model, assume a Gaussian intrachain PDF.[52] These conventional models are clearly inadequate for chains with a non-Gaussian structure. For the case of polymers in deformation and flow, scattering becomes anisotropic due to preferential stretching and orientation of chains. Typical analyses for anisotropic scattering compute low-dimensional descriptors of the scattering anisotropy, providing Fourier-space measures that must be interpreted by using a material-specific model. Previous scattering analyses to extract information regarding polymer configurations in flow have been limited to primitive reduced-dimensional quantification of scattering anisotropy (e.g., anisotropy parameters)[53] or eigenfunction expansion methods (e.g., spherical harmonics)[54,55] which require a number of physical assumptions to map the resulting scattering coefficients to real-space structure. For example, the spherical harmonic expansion (SPE) approach of Chen and co-workers[56−58] describes the scattering through a complete set of Fourier-based spherical harmonic amplitude coefficients. In principle, the resulting q-dependent harmonic coefficients represent specific scattering symmetries and thus contain a unique real-space interpretation. However, doing so requires collapsing the coefficients onto a real-space PDF function, which so far has been assumed to be Gaussian. More recent models attempt to describe anisotropic polymer scattering using a scattering form factor from a thermodynamically consistent connected-rod chain model;[59] however, this model

https://doi.org/10.1021/acs.macromol.4c01169
Macromolecules 2024, 57, 9518−9535

also assumes a particular form of the chain configuration that may fail for sufficiently nonlinear deformations.

From this summary, we see that there is a need for methods to analytically quantify the non-Gaussian PDF of polymers that can be easily extracted from experiments and simulations. In addition to their utility in the analysis of scattering, such methods could be useful in developing structure−property relations for non-Gaussian polymers. For example, there has been significant effort in trying to express the non-Gaussian nature of polymer conformations analytically by calculating their higher-order moments.[3,60,61] Moments are attractive as low-dimensional descriptors of non-Gaussian distributions and can be used to calculate transport properties including mechanical stresses.[62] In this work, we attempt to develop a generally applicable mathematical framework to "fingerprint" non-Gaussian features of polymer conformations that can be used to extract moments of a non-Gaussian polymer PDF using both real-space and Fourier-space (scattering) data. Toward this aim, the Gram−Charlier (G-C) expansion is a valuable mathematical technique used to approximate unknown probability distribution functions by expanding around a reference normal (Gaussian) distribution, offering a more detailed characterization of the distribution shape. This method was first used in the realm of polymer physics by Montroll[63] to calculate higher-order moments of the distribution of end-to-end vectors of a chain on a square lattice. More recent works by Yoon and Flory[60] and Carmichael[64] utilized the G-C analysis to describe non-Gaussian end-to-end distributions from Monte Carlo simulations. In this work, we develop the mathematical analysis required to apply the G-C analysis to describe segment density distributions in both real space (measured from molecular simulation) and Fourier space (measured from scattering) and validate the ability of the analysis to provide identical descriptions of the PDF in either representation. Then, as initial motivating demonstrations, we apply the analysis to two specific cases of non-Gaussian conformations: sequence-defined biopolymers at equilibrium (in which heterogeneous polymer−polymer interactions induce non-Gaussian chain conformations) and flexible linear polymers in flow (in which nonlinear deformations produce an anisotropic non-Gaussian PDF).

THEORY

Describing Polymer Configuration Distributions Using Moments. We seek a mathematical framework to describe complex configuration distributions of individual polymer chains that is agnostic to the details of their chemistry, topology, or mechanical and thermodynamic behavior so that it can be generally applicable to a number of contemporary polymers, processes, and measurement methods. Such distributions could be based on a number of possible descriptors of the chain conformation. One possibility is to describe configurations based on the spatial distribution of the segments about the center of mass, also referred to as the segment or pair density probability distribution function $\psi(r)$, where r is the Euclidean distance from the center of mass of the polymer. This quantity is easily accessed in both molecular simulations and experimental measurements, including small-angle scattering. It is also used in molecular theories to compute various properties, such as hydrodynamic interactions,[65,66] and so is a natural choice for developing structure−property relationships. One might consider alternatives for this choice. For example, the distribution of end-to-end vectors $\psi(R_{ee})$ is easily measured in molecular simulation but is more difficult to access in experiments—a notable exception is double electron−electron resonance (DEER) spectroscopy, which was recently used to characterize $\psi(R_{ee})$ of dilute polymers in solution.[41,42,67] Furthermore, R_{ee} is an incomplete descriptor for more complex polymers including branched and topology-defined polymers as well as chemical heteropolymers, whose structure defies description by simple measures of chain length. Nevertheless, one could in principle employ the analysis to follow any distributed measure of the chain configuration.

While the full reconstruction of a 3D segment density distribution from a 2D scattering pattern is mathematically impossible, we propose to use moments of this distribution as a means of reconstruction. The established mathematical development of the density distribution in terms of moments is described in Section S1. In brief, moments (or equivalently cumulants) are low-dimensional descriptors of a probability distribution function and are agnostic to the details of the distribution. In principle, the exact reconstruction of a distribution function requires measuring an infinite set of moments or cumulants. However, there exist well-established statistical methods whereby the exact distribution function can be expressed by expanding the summation of moments around a reference distribution. In doing so, the exact moment generating function is efficiently approximated using a relatively small number of moments or cumulants, allowing the entire unknown distribution function to be approximated using a small set of descriptors.

One such method, which we will employ exclusively in this work, is the Gram−Charlier (G-C) expansion method[68,69] which allows one to extract moments and cumulants quickly from experiments and simulations, providing physically meaningful and interpretable information regarding the polymer configuration, while remaining indifferent to the precise shape of the underlying distribution. The G-C expansion (Section S1) uses the Hermite polynomials as a natural orthogonal basis for the expansion of a linear combination of increasing order differentiations of a reference normal distribution. The weights (coefficients) for these Hermite polynomials are found to be the cumulants of the original unknown distribution. Thus, the Gram−Charlier expansion provides a route to reconstruct an unknown distribution through estimation of a small set of cumulants that can be directly quantified from the data.

Thus, we see that the general problem of measuring the complete density distribution of a polymer chain (or an ensemble of chains) can be reduced to the problem of measuring the series of moments of the distribution. We thus posit that the set of moments $\{\mu_n\}$ or cumulants $\{\kappa_n\}$ of $\psi(r)$ provides a robust mathematical "fingerprint" of arbitrarily complex polymer configurations, an idea that we will begin to explore in this work. In particular, we propose that such a description is particularly well-suited for topologically or chemically complex polymers at equilibrium as well as for polymers experiencing nonlinear deformations. In all these cases, we expect that $\psi(r)$ will differ significantly from the Gaussian distribution that is typically expected for linear homopolymers at equilibrium or in linear deformations which is typically assumed in most analyses of polymer structure. The idea is to approximate the unknown non-Gaussian $\psi(r)$ using

https://doi.org/10.1021/acs.macromol.4c01169
Macromolecules 2024, 57, 9518−9535

the Gram−Charlier approach in terms of a reference Gaussian polymer chain and use this to develop a fitting scheme for the scattering intensity where the fit parameters are the higher-order cumulants of $\psi(r)$.

The adaptation of the Gram−Charlier expansion scheme to the segment density distribution has been outlined in detail in Section S1. The final analytical expression for the one-dimensional G-C expansion for the unknown chain PDF in terms of its cumulants and Hermite polynomials is

$$\psi(x) = \frac{1}{\sqrt{2\pi}\sigma}\exp\left[-\frac{x^2}{2\sigma^2}\right]\left[1 + \frac{\kappa_4}{4!\sigma^4}He_4\left(\frac{x}{\sigma}\right) + \frac{\kappa_6}{6!\sigma^6}He_6\left(\frac{x}{\sigma}\right) + \frac{\kappa_8}{8!\sigma^8}He_8\left(\frac{x}{\sigma}\right) + \dots\right] \quad (1)$$

where the normal distribution $\phi(x)$ is the leading term of the expansion and the corrections to this are the higher-order cumulants of the unknown PDF normalized by the standard deviation of the normal distribution. For the use of integral calculations to follow, $\psi(x)$ is normalized to give the final form of the chain PDF as

$$\psi(x) = \frac{1}{\sqrt{2\pi}\sigma}\exp\left(-\frac{x^2}{2\sigma^2}\right)\frac{24\sigma^8}{24\sigma^8 + 12\kappa_4\sigma^4 + 4\kappa_6\sigma^2 + \kappa_8 + \dots} \times \left[1 + \frac{\kappa_4}{4!\sigma^4}He_4\left(\frac{x}{\sigma}\right) + \frac{\kappa_6}{6!\sigma^6}He_6\left(\frac{x}{\sigma}\right) + \frac{\kappa_8}{8!\sigma^8}He_8\left(\frac{x}{\sigma}\right) + \dots\right] \quad (2)$$

The normalization prefactor will change based on the number of terms kept in the expansion, and eq 2 shows the normalization for terms up to $n = 8$.

Small-Angle Scattering: The Fourier-Space Gram−Charlier Expansion. We use the Gram−Charlier representation of the chain PDF (eq 2) to derive an analytical form of the scattering intensity for a polymer with general non-Gaussian conformation distribution. In the limit of an isolated polymer chain, the (one-dimensional) scattered intensity is given by a Fourier transform of the chain segment PDF as follows:

$$I(q) = K\left(1 + \int \psi(x)e^{-iqx}\mathrm{d}x\right) \quad (3)$$

Substituting eq 2 for $\psi(x)$ from yields the Fourier-space representation of the Gram−Charlier expansion. Fortunately, due to the properties of the Gram−Charlier series, the Fourier transform can be calculated analytically to arbitrary n, yielding (for the $n = 8$ case)

$$I(q) = K\left(1 + \exp\left(-\frac{q^2\sigma^2}{2}\right)\frac{24\sigma^8}{24\sigma^8 + 12\kappa_4\sigma^4 + 4\kappa_6\sigma^2 + \kappa_8}\left[1 + \frac{4\kappa_4}{4!\sigma^4}(3 - 12q^2\sigma^2 + 4q^4\sigma^4) + \frac{8\kappa_6}{6!\sigma^6}(15 - 90q^2\sigma^2 + 60q^4\sigma^4 - 8q^6\sigma^6) + \frac{16\kappa_8}{8!\sigma^8}(105 - 840q^2\sigma^2 + 840q^4\sigma^4 - 224q^6\sigma^6 + 16q^8\sigma^8)\right]\right) \quad (4)$$

where q is the (1D) scattering wavevector, K is a q-independent amplitude factor which is system-specific and depends on the concentration and scattering length densities of polymer and solvent, $\sigma = \mu_2 = \frac{2}{\sqrt{3}}R_g$ is the (Gaussian) size of the polymer chain for an isotropic chain configuration, and $\{\kappa_n\}$ are the higher-order cumulants that quantify the non-Gaussian characteristics of the conformation distribution. For example, κ_4 is the fourth cumulant and is related to the fourth moment by $\mu_4 = 3\mu_2^2 + \kappa_4$. In the work to follow, eq 4 will be used to fit various 1D averages of predicted or measured scattering intensities. Further details of the G-C analysis of polymer scattering and how it is applied to both simulated and experimentally measured scattering data will be discussed in the applied case studies to follow.

CASE STUDY I: INFERRING NONIDEAL POLYMER CONFORMATIONS AT EQUILIBRIUM

Ideal flexible polymers are expected to exhibit a Gaussian segment density distribution at equilibrium, and this ideal model adequately captures the long-wavelength structure observed for equilibrium homopolymers in the melt and in solution.[2,35] However, polymers with more complex chemistry can possess significant deviations from ideal Gaussian conformations at equilibrium. Examples include heteropolymers—such as random, blocky, or sequence-defined copolymers—as well as topology-defined polymers including branched, star-like, dendrimeric, and bottlebrush architectures, especially in good solvents where excluded volume effects result in non-Gaussian density profiles near the backbone.[70] We hypothesize that the G-C analysis presented here can be useful to mathematically describe the non-Gaussian conformations of such nonideal polymers. In particular, the analytical result of eq 4 provides a route to quantify the non-Gaussian moments of the PDF directly from small-angle scattering data. In this section, we test this idea for a model class of sequence-defined polypeptoid heteropolymers that have been previously demonstrated by both molecular simulation and advanced electron paramagnetic resonance spectroscopy experiments to possess non-Gaussian conformations due to intramolecular associative interactions.[71]

Non-Gaussian Behavior of Sequence-Defined Polypeptoids. DeStefano et al.[71] synthesized a library of sequence-specific polypeptoids comprising hydrophilic residues (*N*-methoxy ethyl glycine), hydrophobic residues (*N*-phenethyl glycine), and terminal spin labels (nitroxide radical-based TEMPO spin probes) with precisely patterned arrangement of the monomers to investigate the influence of hydrophobic sequence on the chain conformation as shown in Figure 1a. For this work, we examine three of these polypeptoid sequences with a degree of polymerization DP = 20 monomers. Namely, "0H", "3H," and "Mid" have the same degree of polymerization with molecular weights ranging from 2500 to 2800 g/mol, but varying the number and placement of the hydrophobic moieties. Sequence "0H" has no hydrophobic groups on the chain, "3H" has three hydrophobic groups located at each chain end, while "Mid" has six hydrophobic groups placed in the middle of the chain. In previous work, it was shown that controlling the monomer sequences of these polypeptoids alters their conformational landscapes, resulting in significant deviations from ideal chain statistics. In particular, the end-to-end distance distribution $P(R_{ee})$ of the sequences was experimentally estimated using double electron−electron resonance (DEER) spectroscopy, which is a

https://doi.org/10.1021/acs.macromol.4c01169
Macromolecules 2024, 57, 9518−9535

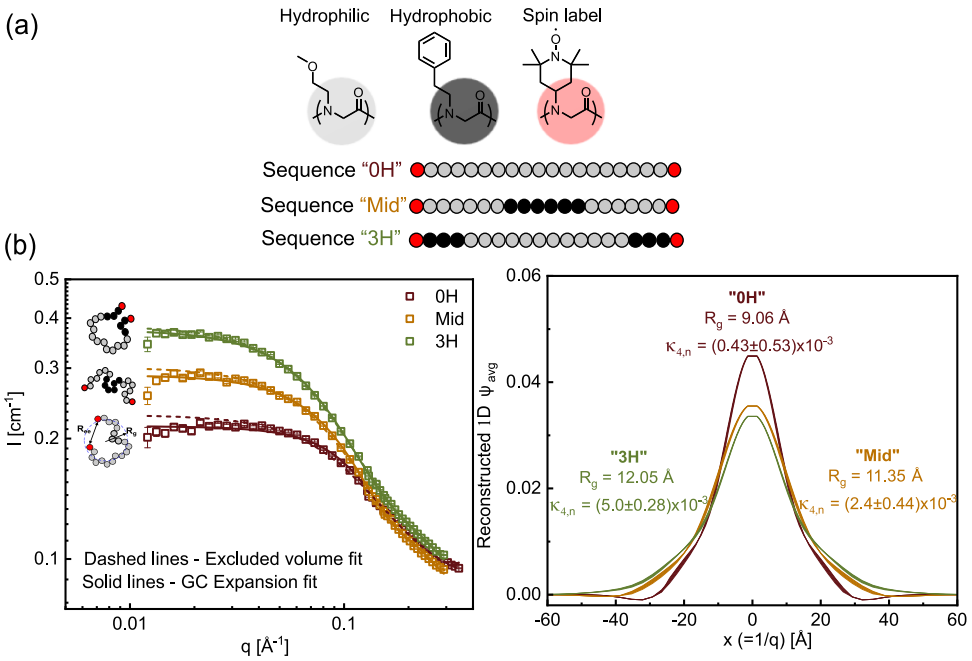

Figure 1. (a) Different polypeptoid sequences with varying hydrophobe content and patterning along the polymer backbone. (b) Left: radially averaged SANS spectra showing fits to the 1D-Gram−Charlier expansion (solid line) and excluded volume model (dashed line) for the different peptoid sequences; right: reconstructed real-space segment density PDFs from the corresponding G-C fit parameters ($R_g = \frac{\sqrt{3}}{4}\sigma$ and higher-order cumulants $\{\kappa_n\}$). The shaded area around the curves represents the 95% confidence intervals of the reconstructed 1D real-space segment density distribution. Reported fourth-order cumulants were normalized by σ.

pulsed electron paramagnetic resonance technique that measures distances between spin labels, thus providing access to conformational distributions.

The reported findings from DEER indicated that the hydrophobic patterned sequences possess non-Gaussian conformations, with increasing non-Gaussian character in the order "0H" < "Mid" < "3H". That is, hydrophobic intramolecular associations drive increasing nonideal conformations, and this nonideal behavior is enhanced when the hydrophobic moieties are proximal to the ends of the chain. This is more clearly exemplified by comparing the second moment of $P(R_{ee})$, which gives an estimate of the RMS end-to-end distance $\langle R_{ee}^2 \rangle^{1/2}$ (refer to Figure S1). The smaller $\langle R_{ee}^2 \rangle^{1/2}$ seen for the "3H" polypeptoid compared to the compositionally equivalent "mid" sequence was rationalized by hypothesizing that end associations more significantly confine the chain conformation, whereas in the "Mid" configuration, the chain ends are more free to sample a variety of configurations resulting in decreased skewness (increased symmetry) than "3H" but more than the homopolymer-like "0H". The non-Gaussian behavior of the polypeptoids therefore arises from a combination of intramolecular associations and sequence-defined chemistry. The transition from a Gaussian-coil-like structure to more nonclassical conformations upon patterning hydrophobes in the peptoids was confirmed by DEER, establishing the foundation for this case study. To complement the DEER measurements, we applied G-C analysis on the scattering data collected for these systems. This approach allowed us to discern trends in the segment density distribution of the sequences while remaining neutral with the specifics of polymer chemistry.

Gram−Charlier Analysis Applied to Equilibrium SANS from Polypeptoids. In the Theory section, we showed that the Gram−Charlier expansion provides analytical results for the scattered intensity from an ensemble of isolated individual chains (eq 4). As such, the G-C analysis can be used as a fitting tool for one-dimensional averaged scattering intensity data to directly quantify deviations from Gaussian conformations. To this end, we applied eq 4 to 1D radially averaged SANS measurements of the sequence-defined peptoids. The SANS measurements were taken at the extended q-range small-angle neutron scattering diffractometer instrument (EQ-SANS, BL-6) at the Oak Ridge National Laboratory (ORNL) Spallation Neutron Source.[72,73] Purified and filtered polypeptoid samples were dissolved at 25 mg/mL ($\approx 0.07c^*$) in a 50−50 mixture of deuterated tetrahydrofuran and deuterium oxide (by volume). The three 20-mer polypeptoid samples ("0H", "Mid", and "3H") were loaded into quartz banjo cells with a 2 mm path length and equilibrated to 20 °C. 2D scattering patterns were taken at two sample-to-detector distances (4 and 2.5 m), both with a neutron wavelength band defined by a minimum wavelength of 2.5 Å. Data were reduced to an isotropic scattering pattern using standard python scripts.[74,75] Measured scattering intensities were calibrated using a Porasil B standard and corrected to remove scattering of the empty banjo cell. The resulting 1D scattering spectra are plotted for the three polypeptoid sequences in Figure 1b.

We note two key assumptions we make in applying our analysis (specifically, the application of eq 4) to the measured scattering from peptoid solutions. First, we assume that the scattering interference arising from intermolecular interactions is negligible; that is, the solutions are sufficiently dilute. Here, SANS from the peptoid samples was measured at a concentration of $0.07c^*$, where c^* is the overlap concentration estimated from the measured R_g values, such that any intermolecular interactions are minimized. Second, we assume

https://doi.org/10.1021/acs.macromol.4c01169
Macromolecules 2024, 57, 9518−9535

that the radial scattering length density (SLD) profile that determines the measured scattering is directly proportional to the segment density PDF of the polymer, such that eq 4 can be directly applied. While eq 4 is exact for a homopolymer, this relationship might not hold for a heteropolymer like the peptoid sequences used in this study, which contain chemically distinct monomers with different SLDs. To check the approximate accuracy of this assumption for heteropolymers, Section S2 extends eq 3 to the case of a polymer with heterogeneous monomer SLDs. For the specific monomer SLDs of the present peptoids (see Section S2), we confirmed that heterogeneities in the SLD distribution in this specific case do not significantly alter the predicted scattering or values of the higher-order moments extracted from the G-C analysis relative to the case of a homopolymer (Table S3).

To demonstrate the utility of the G-C analysis of the SANS data developed here relative to conventional models, we compare the G-C fits of the data to a more conventional excluded volume (EV) polymer model where the form factor and the R_g can be expressed as[76]

$$I(q) = 2\int_0^1 (1-x)\exp\left[\frac{-q^2R_g^2}{6}x^{2\nu}(2\nu+1)(2\nu+2)\right]dx \tag{5}$$

Here, ν is the excluded volume parameter (which is related to the high-q Porod exponent, $m = 1/\nu$), and R_g is the radius of gyration. A fit of eq 5 to the polypeptoid SANS data (dashed lines) with adjustable values of R_g and ν (with best-fit values reported in Section S2) does a relatively poor job describing the data, especially in the low-q region, and thus overestimates the R_g of the polymer (refer to Table S1). By contrast, the G-C analysis (eq 4) provides an excellent quantitative description of the measured scattering when fitted to the scattering profiles (solid lines). Notably, the G-C analysis is able to better capture the low-q scattering intensity, as well as the sharper transition between the low-q plateau and moderate-q shoulder exhibited for all of the polymer sequences. The G-C analysis therefore provides quantitative information about the distribution of R_g through higher-order cumulants $\{\kappa_n\}$. The fitting using eq 4 was constrained to a range of $q < 0.3\text{Å}^{-1}$ to obtain a satisfactory fit, since the Gram−Charlier expansion fails to describe higher-q features where intrasegmental correlations are probed. This limitation does not impact the ability of the expansion scheme to extract the non-Gaussian characteristics of the chain, which is primarily manifested through κ_4 and is insensitive to the scattering data beyond $q \sim 0.1\text{Å}^{-1}$. Similarly, the higher-order cumulants κ_6 and κ_8 exhibit nonzero values in a pattern consistent with increased non-Gaussian chain conformations from "0H" to "Mid" to "3H" (Table S2).

The radius of gyration R_g of the polymer chain can also be independently evaluated using a conventional Guinier analysis of the low-q scattering using

$$\lim_{qR_g \ll 1} \ln I(q) = \ln I_0 - \frac{q^2R_g^2}{3} \tag{6}$$

The values of R_g obtained as a fitting parameter from the G-C analysis are closer to those obtained from the Guinier analysis, whereas the EV model fit significantly overpredicts the values of R_g (refer to Table S1). As the hydrophobes are placed closer to the chain ends, the polymers tend to assume a compact ring-like shape, producing an increase in R_g and a subsequent decrease in R_{ee} as seen for "3H". By contrast, placing the hydrophobes in the center of the chain causes the ends to be more free and collapse in the center, leading to smaller R_{ee} than "0H" and lower R_g than "3H". More importantly, the presence of non-Gaussian conformations is reflected in the nonzero higher-order cumulants, such as κ_4 shown in the labels in Figure 1b. As expected from the DEER measurements in Figure 1b, the value of κ_4 changes from almost zero for the homopolymer "0H" in the absence of hydrophobic moieties (indicating near-Gaussian conformations) to increasingly nonzero values when hydrophobes are introduced in the sequence, reflecting the increasing non-Gaussian nature of the chain conformations.

Furthermore, because of the 1:1 interchangeability of the cumulants between the real-space and Fourier-space descriptions of the G-C expansion described in the Theory section, the G-C analysis of polymer scattering provides a direct mathematical reconstruction of the inferred real-space segment density PDF, which can be used to visualize the non-Gaussian features of the 1D PDF (Figure 1b). Specifically, as captured by the relative values of R_g and κ_4, the intramolecular PDF broadens and develops a longer non-Gaussian tail as hydrophobic moieties are introduced to the peptoid sequence and as these hydrophobes are placed proximal to the chain ends. We note that for the "0H" sequence, the inferred PDF exhibits anomalous negative values at longer distances from the chain center—this arises because the fitting scheme implemented does not constrain $\psi_{avg}(r)$ to be strictly positive. Although this spurious feature does not affect the comparisons made in the present study, the G-C expansion and fitting schemes could be modified to include a constraint that penalizes negative values of $\psi(x)$ as proposed previously.[77] These negative values arise from the truncation of the G-C series, and as a result, such constraining will be truncation-dependent and therefore *ad hoc*, and so we choose not to include it in this work.

Overall, through this example, we demonstrate that the application of the G-C analysis to equilibrium small-angle scattering can be used to test for nonideal polymer conformations in a model-independent manner that is agnostic to the details of polymer chemistry. More importantly, the G-C analysis provides unambiguous quantification and interpretation of non-Gaussian features of the intramolecular PDF, including the ability to fully visualize the PDF as expressed by the set of extracted cumulants. For the specific case of the sequence-defined polypeptoid heteropolymers examined here, the results provided an interpretation for the differences in intramolecular structure that required no assumptions about the specific molecular configuration and that qualitatively reproduces the configurational information obtained through other independent experiments (in this case, $P(R_{ee})$ from DEER measurements). Because of the different nature of $\psi_{avg}(r)$ (which encodes the density of individual polymer segments around the center of mass) and $P(R_{ee})$ (which encodes pair distances between the chain ends), the two measurements defy direct quantitative comparisons. For that, we turn to an additional case study where the scattering "data" are produced from molecular simulation; that is, the exact PDF represented by the scattering is known, and therefore, the accuracy and precision of the G-C analysis can be more quantitatively established.

https://doi.org/10.1021/acs.macromol.4c01169
Macromolecules 2024, 57, 9518−9535

CASE II: CHARACTERIZING NONLINEAR POLYMER DEFORMATIONS IN FLOW

To demonstrate that the Gram−Charlier expansion can be extended to describe non-Gaussian polymer conformations for nonequilibrium systems, we applied the analysis to molecular simulations of polymers undergoing nonlinear deformations in shear flow. The influence of flow introduces deviations in the conformational distributions of polymer chains from ideal Rouse or Zimm statistics due to factors such as nonlinear stretching, hydrodynamic interactions, excluded volume, and frictional drag. In addition, shear flow produces time-fluctuating combinations of stretching and rotation that should be evident in the time-averaged PDF. To test this idea, we apply the G-C analysis to simulated data on isolated polymers in shear flow. Applying the method to simulations presents a number of advantages for an initial demonstration of the method. First, because the "ground truth" of the simulated data is known, we can validate the Fourier-space representation of the method to be applied to scattering by comparing cumulants extracted from the "known" real-space chain segment PDF (by fitting to eq 2) to that extracted from simulations of the scattering intensity (by fitting to eq 4). Second, one can evaluate the convergence and error of the analysis by truncating the cumulant expansion of eq 2 to various terms and also the sensitivity of the analysis to varying amounts of experimentally relevant noise added to the simulated scattering (by adding a random contribution to eq 4). Third, the use of simulated scattering data avoids potential complications associated with experimental material systems and scattering measurements including molecular polydispersity, intermolecular interactions, nonhomogeneous deformations, and measurement resolution. Finally, by connecting the simulations to a specific physical model(s) of polymer mechanics, we can attempt to provide physical interpretability of the resulting cumulants. A thing to note here is that the experimental measurements for polymers in flow have added complexities such as polydispersity and intermolecular interactions, which convolutes the interpretation of the analysis. Furthermore, in nearly every sample environment for generating sufficiently large strain rates to produce non-Gaussian conformations, there are inherently gradients in the strain rate that must be considered in the interpretation of the scattering intensity, which typically averages over these gradients. We feel that a thorough investigation of the effects of these experimental factors and artifacts on the G-C analysis requires a more extensive experimental study beyond the scope of the current work.

An important consideration in the application of the G-C analysis to deformed polymers is that the current form of the expansion used is supported only on a one-dimensional space of the polymer conformation. As such, to apply the current analysis to flowing polymers—which possess an anisotropic three-dimensional PDF—requires one-dimensional preaveraging of the PDF. In the analysis to follow, this will be performed by computing various projections of the fully 3D PDF (or its equivalent scattering pattern) to a single direction (chosen here to be the flow direction). This procedure will necessarily introduce errors between the apparent 1D values of the cumulants and their "true" 3D equivalents. In the analysis to follow, we will evaluate the extent of this error and determine whether the 1D version of the analysis suffices to describe the non-Gaussian structure of the PDF. Ideally, for polymers in deformation, flow, or other situations producing an anisotropic PDF, one would extend the analysis to the multidimensional case. The general procedure for doing so has been outlined in previous works[78] and has been performed to $O(\kappa_4)$. However, extending the analysis to higher-order moments is nontrivial, as the resulting tensorial forms for the cumulants must obey the relevant symmetries of polymer mechanics and rheology (e.g., corotational invariance). As such, we leave a general treatment of the 3D analysis to future work.

Brownian Dynamics Simulations of Isolated Polymers in Shear Flow. In the simulations, a portion of the chain containing several hundred monomers is represented as a bead, and the bead is typically assumed to have point-like dimensions, neglecting its internal structure. The bead is connected to its neighboring beads by springs, which model the entropic elasticity of the chain between the monomers and are considered to be thin and flexible.[79,80] In our coarse-grained Brownian dynamics simulations, only a section of the polymer chain, represented by beads, is tracked (refer to Section S4 for details of the simulation). The number of beads determines the resolution of the system: a higher number of beads provide a greater observed resolution. However, increasing the bead number significantly extends the simulation time. The model employed here neglects excluded volume interactions for computational efficiency. Many forces, such as the spring force, Brownian force, and hydrodynamic interactions, play important roles in the simulation.

Finite Extensibility. Two types of springs are used to model the polymer chain: Hookean springs and finitely extensible nonlinear elastic (FENE) springs. For Hookean springs, $\boldsymbol{F}_{ij}^{s} \cong H\boldsymbol{Q}_{ij}$, where $\boldsymbol{Q}_{ij} = \boldsymbol{r}_i - \boldsymbol{r}_j$ is the extension of a spring between beads i and j. The spring constant H is a measure of the stiffness of the spring and is defined as the magnitude of the spring force F^s required to stretch the spring by one unit of length.[81] FENE springs cannot extend indefinitely beyond their contour length. The relationship between force and displacement for a conventional FENE spring model is defined as[82]

$$\boldsymbol{F}_{ij}^{s} = \frac{H\boldsymbol{Q}_{ij}}{1 - \left(\frac{\boldsymbol{Q}_{ij}}{Q_0}\right)^2} \tag{7}$$

where Q_0 represents the maximal extension of the spring. When the polymer experiences relatively small deformation rates, the resulting deformation between beads is small and polymers with Hookean springs and FENE springs behave similarly. As Q_{ij} becomes larger, the nonlinearity of the FENE spring becomes more pronounced, and differences in behaviors of the two types of springs grow. In the following, we evaluate the degree to which this nonlinearity manifests in the non-Gaussian polymer configuration. To correctly model the molecular weight dependence of the nonlinear polymer deformation, the maximal extension of the FENE spring Q_0 can be described as, $Q_0 = N_{k,s}A_k$, where $N_{k,s}$ is the number of Kuhn steps represented by a single spring and represents the average length of a flexible segment and A_k is the Kuhn length. Since polymers with Hookean chains can be infinitely stretched and have no limiting contour length, this parameter only needs to be considered when simulations are conducted with FENE springs. A dimensionless spring stiffness b_s is defined as[82] $b_s = \frac{HQ_0^2}{(k_BT)}$. The spring constant H can be written as[25] $H = \frac{3k_BT}{(Q_0A_k)}$. Using the two previous equations, we obtain

https://doi.org/10.1021/acs.macromol.4c01169
Macromolecules 2024, 57, 9518−9535

$b_s = \frac{3Q_0}{A_k} = 3N_{k,s}$. A dimensionless molecular parameter b_m is defined as $b_m = N_{spr}b_s$, where N_{spr} is the number of springs in the bead−spring model. In the simulations, b_m is held constant across different resolutions for the same size of molecules, while b_s varies based on the number of springs within the model. The two FENE chains investigated in this work have b_m = 3000 and 450, where higher values of b_m represent more extensible chains.

Weissenberg Number. The Weissenberg (Wi) number characterizes the dimensionless deformation rate of a fluid due to shear and is defined here as the product of the shear rate $\dot{\gamma}$ and the Rouse relaxation time λ_R, $Wi = \dot{\gamma}\lambda_R$. The relaxation time for the linear polymer is defined as,

$$\lambda_j = \frac{\zeta}{8H\sin^2(j\pi/2N)} \tag{8}$$

The Rouse relaxation time λ_R is equal to λ_1, the largest normal mode of a Rouse chain. Large values of Wi are expected to correspond to a more pronounced elastic response and a larger deformation of the polymer chain and thus a more nonlinear stretch of the springs comprising the chain. At sufficiently large Wi, linear polymer chains stretch significantly in the flow direction, reducing the probability of bead overlap and making excluded volume interactions negligible.

Polymer Conformational Distributions in Flow from Simulations. Simulations yield a data set comprising bead-to-bead vectors $\{\boldsymbol{r}_{ik}\}$, which are recorded in three dimensions, r_x, r_y, and r_z (Figure 2a). A suitable number of bins is selected

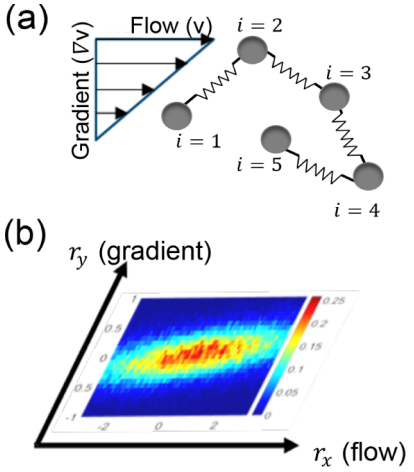

Figure 2. (a) Schematic representation of a coarse-grained polymer chain (here, N = 5 beads) in shear flow. (b) 2D projection of the overall ensemble-averaged chain distribution as an output from the simulations in the flow-gradient plane.

to discretize the range of $\boldsymbol{r}$. Iterating through all values of $\boldsymbol{r}$, we count occurrences within each bin and subsequently normalize the counts to approximate the segment density PDF $\psi(\boldsymbol{r})$. Figure 2b shows the 2D projection of the 3D PDF by taking a slice in the $r_x - r_y$ plane at an r_z value corresponding to the midplane of the simulation. The ensemble-averaged gyration tensor $\boldsymbol{G}$ can also be obtained from the simulations, where $\boldsymbol{G} = \frac{1}{N}\sum_{\nu=1}^{N}\langle \boldsymbol{R}_\nu \boldsymbol{R}_\nu \rangle$ and $\boldsymbol{R}_\nu$ is the bead position vector with respect to the center of mass of the chain. $\boldsymbol{G}$ is related to the radius of gyration through $R_g = tr(\boldsymbol{G})$. For a Rouse chain, this can be analytically calculated using a normal-mode analysis, as shown in eqn. S16. At equilibrium, the configuration is isotropic, and one thus obtains $G_{xx} = G_{yy} = G_{zz} = R_g^2/3$. During flow (in the x-direction), G_{xx} increases in the value, whereas the G_{yy} and G_{zz} either remain identical to their equilibrium values (for the case of a Rouse chain) or decrease to account for compression in the velocity gradient and vorticity directions (for a FENE chain). We define $R_{gx,0} = R_g(Wi = 0)$ as the radius of the gyration of the polymer at equilibrium. Scaling the bead-to-bead vector $\boldsymbol{R}$ with $R_{gx,0}$ therefore provides a measure of the polymer stretch relative to its equilibrium size.

Analysis of BD Simulations of Polymers in Flow. Upon increasing the strength of the flow (increasing Wi), the overall width of $\psi_{avg}(r)$ increases, indicating chain stretch due to flow. This is represented in Figure 3, where the PDF has been averaged over the r_y and r_z directions to produce a quasi-1D PDF along the flow (r_x) direction. Here, the bead-to-bead distance has been normalized by $R_{gx,0}$ such that $r_x = 1$ represents the width of the PDF at equilibrium to emphasize the stretching of the chain relative to the equilibrium value. As expected, increasing Wi increases the nominal stretch on the chain (i.e., the PDF becomes broader). Simultaneously, the non-Gaussian character of PDF increases. For the Rouse chain simulations, this is evident in the emergence of a long tail in the distribution at relatively large r_x. This behavior is exaggerated for a FENE chain (Figure 3b). Additionally, the FENE simulations develop nearly flat-shaped peaks when Wi > 10. This suggests that upon increasing the flow strength the nonlinear chain extensibility begins to dominate the overall conformational deformation of the chain. However, we note in Figure 3c that increasing amounts of non-Gaussian character are even evident for simulations of Rouse chains and that this becomes more exaggerated for finer-grained simulations involving increasing numbers of beads, where the PDF exhibits an increasingly sharp central peak while maintaining a relatively flat "long tail".

This last observation that the non-Gaussian behavior is evident with increasing chain stretching even for a Rouse chain may be surprising and counterintuitive since the normal modes that represent the Rouse chain each follow a Gaussian distribution. However, this behavior can be explained when one considers how the "total" ensemble-averaged segment density PDF of a bead−spring chain relates to the distribution of individual bead pairs (i.e., the individual parts of the chain). Real polymers (corresponding to the large-N limit of the bead−spring model) have a wide distribution of relaxation modes, whereby the longer (slower) modes arise from the motion of large molecular chain segments and the short (faster) modes are associated with the segment-scale dynamics.[83] The relaxation spectrum therefore reflects the polymer microstructure in a complex manner. There has been significant interest in establishing a direct correlation between the relaxation spectrum and molecular structure to develop better mechanistic insights. For a Rouse chain, this ensemble-averaged segment density distribution can be expressed as the weighted sum of the various segmental modes, each characterized by a distinct length scale.

For a given number of beads in the BD simulations, we can track this distribution of the various deformation modes by observing individual bead pairs, as shown in Figure 5 for a five-

https://doi.org/10.1021/acs.macromol.4c01169
Macromolecules 2024, 57, 9518−9535

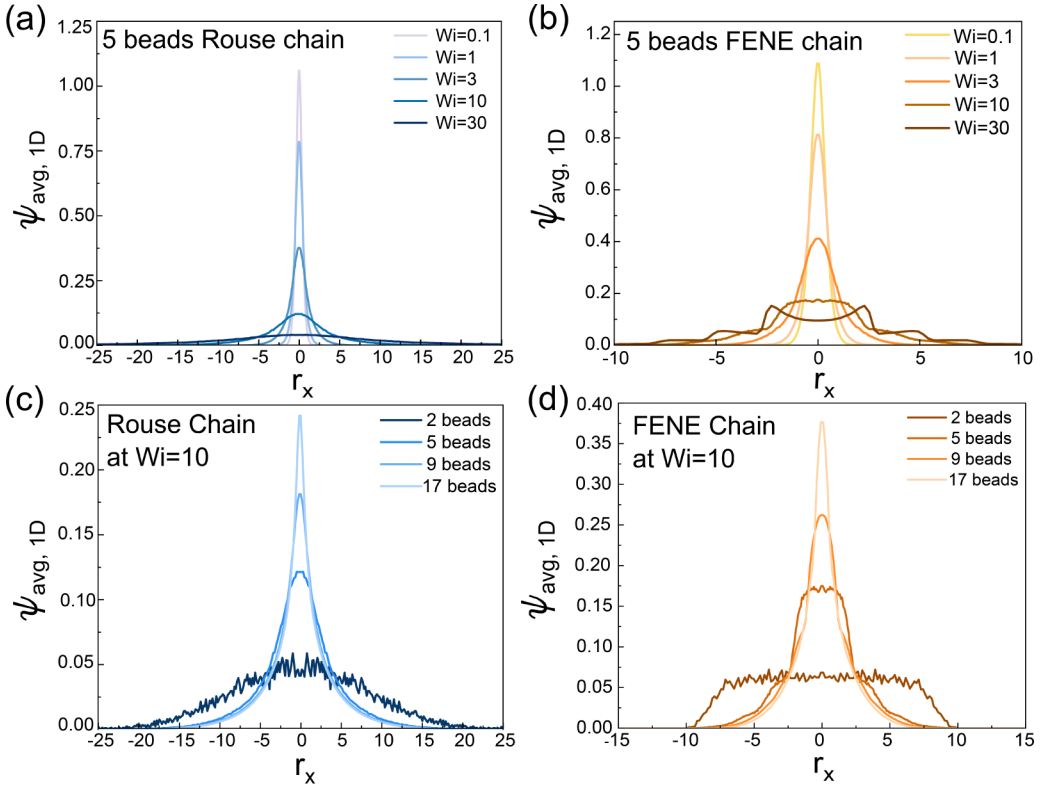

Figure 3. Top panel: average 1D segment density PDF in 1D integrated over r_y and r_z directions for a five-bead polymer chain as a function of *Wi* for (a) Rouse and (b) FENE $b_m = 450$ chains. Bottom panel: average chain PDF in 1D integrated over r_y and r_z directions for a five-bead polymer chain at $Wi = 10$ as a function of chain discretization (number of beads, N) for (c) Rouse and (d) FENE $b_m = 450$ chains.

bead Rouse chain at $Wi = 10$. For example, we observe Gaussian PDFs for each of the individual bead pairs ψ_{ij}, for example, those at the end of the chain ($ij = 12$) or in the middle of the chain ($ij = 23$). However, because the overall chain PDF comprises a weighted sum over all individual bead pairs, the resulting sum of Gaussians with differing variance is non-Gaussian (Figure 4). At moderate *Wi*, this non-Gaussian behavior increases with increasing *Wi* because of the increasing dispersity of bead-pair stretches as the rate of stretching begins to differentially exceed the time scales associated with the various normal modes, in essence, causing different length scales of the chain to experience different "effective" *Wi*. The middle segment of the chain, representing the slower modes, contributes to the tails of the distribution, while the faster modes, located at the ends of the chain, primarily influence the peak of the distribution. We emphasize that such non-Gaussian behavior is intrinsic to any multibead model at moderate *Wi*, even when effects such as excluded volume, chain extensibility, or hydrodynamic interactions are ignored (as is the case in the Rouse model).

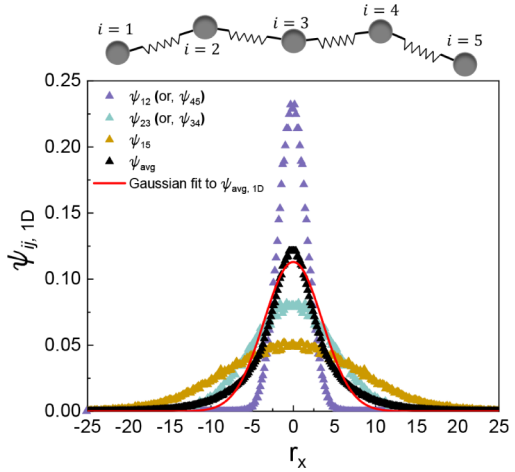

Figure 4. Different bead-pair distributions $\psi_{ij,1D}$ for a five-bead Rouse (or Hookean) chain at $Wi = 10$ shown in symbols and a Gaussian fit to the overall chain avg $\psi_{avg,1D}$ shown in a red line indicating that even Rouse chains do not follow a Gaussian distribution in strong shear flows.

As mentioned previously, non-Gaussian features become evident when additional physics such as nonlinearities in springs are included. For the case of a FENE chain, the effect of finite extensibility on the segment density PDF is to cut off the "long tail" of the distribution described previously due to the imposition of a maximum separation of beads, resulting in the flat and sharply decaying peaks seen in 5. We will later see through the Gram−Charlier analysis that this behavior results in qualitatively different behaviors of the higher-order moments of the chain PDF, thus helping one to identify signatures of the force−extension behavior for different polymers in high shear flows.

Predicting Scattering from Simulated Chain Segment PDFs in Flow. We can model the scattering of dilute linear polymer chains as that arising from N infinitesimal point sources of scattering length connected by $N - 1$ elastic springs with the same scattering length density as the solvent. Clearly, this approach will fail for sufficiently large q-values (small distances) but should retain the relevant scattering features at

https://doi.org/10.1021/acs.macromol.4c01169
Macromolecules 2024, 57, 9518−9535

smaller q-values due to the connectivity of the chain. Formally, we expect such a description to be valid for q-values where $qb \ll 1$, where b is the Kuhn length of the chain. In this case, the distribution of the scattering density is proportional to the chain segment density PDF simulated using Brownian dynamics. In general, the scattering intensity from a single isolated bead−spring chain with a known PDF is determined by a Fourier transform of the time-averaged PDF of each individual bead pair $\psi_{ij}(\mathbf{r})$. The general expression for the coherent scattering intensity from polymer chains is as follows:

$$\overline{I(\mathbf{q})} = cP(\overline{\mathbf{q}})S(\mathbf{q}) + bkgd = \phi(\Delta\rho)^2 V_p P(\overline{\mathbf{q}})S(\mathbf{q}) + bkgd \tag{9}$$

where I_0 is a constant dependent on the material composition and concentration, and the overbar represents an ensemble average of the quantity, and $bkgd$ is the incoherent background intensity. Eq 9 assumes that intramolecular and intermolecular contributions are linearly separable—this assumption will be valid as long as individual polymer molecules are non-overlapping. The prefactor is dependent on the scattering length density difference (i.e., contrast) in the system between the object (polymer) and the surrounding media (solvent) $(\Delta\rho)^2$, the volume fraction of polymer segments ϕ, and the volume of an individual polymer V_p. $P(\mathbf{q})$ is the form factor which is related to the segment density PDF polymer and describes the intraparticle scattering correlations, whereas $S(\mathbf{q})$ is the structure factor that describes intermolecular interactions (i.e., how individual objects are positioned and oriented relative to each other). We emphasize that $\mathbf{q}$ is a vector, and so the scattering in general will depend on the direction of q relative to the local orientation of the material. The simulations considered here involve single polymer chains (i.e., infinitely dilute conditions), and so $S(\mathbf{q}) = 1$. Without accounting for the prefactor which is specific to a system and will not change with orientation of the object, we can therefore approximate the intensity by $P(\mathbf{q})$ which is related to the chain PDF for a system of point scatterer beads as

$$\begin{aligned} P(\mathbf{q}) &= \frac{1}{N^2}\sum_{i,j}^{N}\langle \exp(-i\mathbf{q}\cdot\mathbf{r})\rangle \\ &= \frac{1}{N^2}\sum_{i,j}^{N}\int \exp(-i\mathbf{q}\cdot\mathbf{r})\psi_{ij}(\mathbf{r})\mathrm{d}\mathbf{r} \\ &= \frac{1}{N^2}\left(N + \sum_{i,j}^{N}\int \exp(-i\mathbf{q}\cdot\mathbf{r})\psi_{ij}(\mathbf{r})\mathrm{d}\mathbf{r}\right) \end{aligned} \tag{10}$$

where $\mathbf{r_{ij}}$ is the vector between beads i and j, N is the number of beads per chain, and $\psi_{ij}(\mathbf{r_{ij}})$ is the PDF of individual bead pairs. Eq 10 includes scattering contributions from the individual beads of the chain as well as the scattering interference between pairs of beads. However, this process can become exceedingly computationally demanding, especially with a large number of beads, as it necessitates accounting for interactions between each pair of beads. An alternative approach is to use the weighted sum of these individual bead-pair distributions, that is, $\psi_{avg}(\mathbf{r})$, directly using

$$P(\mathbf{q}) \approx \frac{1}{N^2}\left(N + N(N-1)\int \exp(-i\mathbf{q}\cdot\mathbf{r_{ij}})\psi_{avg}(\mathbf{r})\mathrm{d}\mathbf{r}\right) \tag{11}$$

The scattering patterns calculated from eq 11 using simulated data sets can effectively capture the anisotropy of the chain configuration in higher Wi flows when the chains get stretched in the flow direction (Figures 5 and 6a). Differences in the

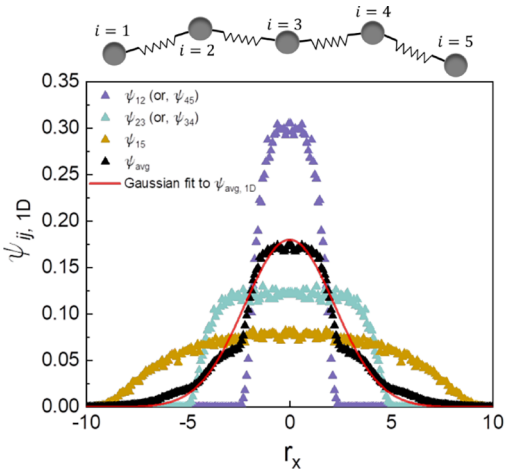

Figure 5. Different bead-pair distributions $\psi_{ij,1D}$ for a five-bead FENE $b_m = 450$ chain at $Wi = 10$ shown in symbols and a Gaussian fit to the overall chain avg $\psi_{avg,1D}$ shown in a red line indicating the highly non-Gaussian behavior of FENE chains as a result of nonlinearity of the springs.

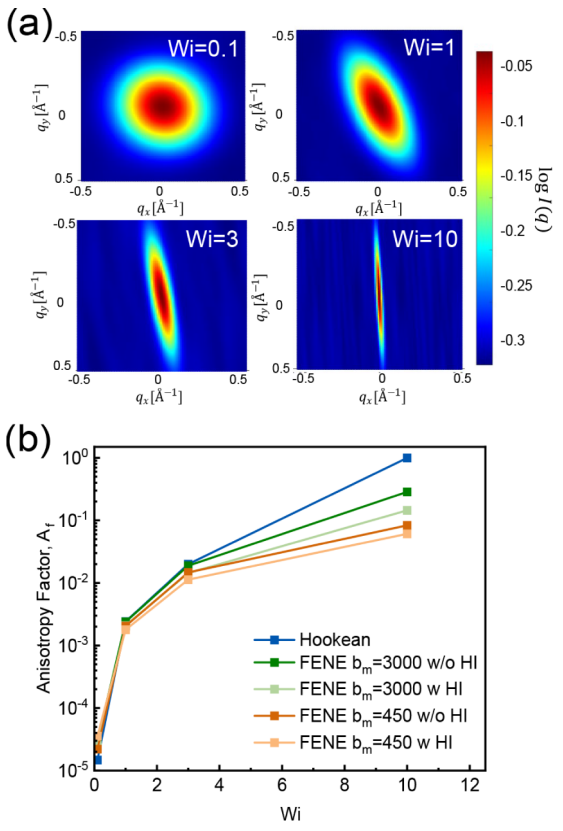

Figure 6. (a) Predicted 2D scattering plots for a five-bead Hookean chain at different Wi flows. (b) Anisotropy factors calculated from annularly averaged data using eq 12 for a chain ($N = 5$) with varying levels of finite extensibility as a function of Wi.

https://doi.org/10.1021/acs.macromol.4c01169
Macromolecules 2024, 57, 9518−9535

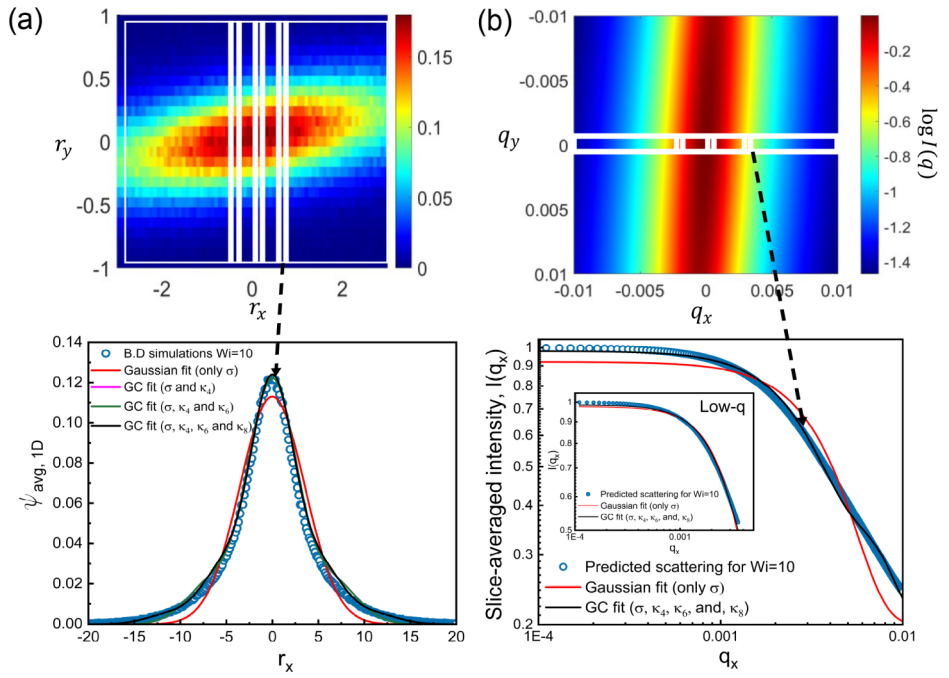

Figure 7. (a) Top: 2D projection of the average 3D segment density distribution (ψ_{avg}) by integrating over the vorticity (z-) direction; bottom: 1D projection of ψ_{avg} in the flow direction obtained by integrating the 2D projection over the gradient (y-) direction with the Gram−Charlier expansion fit (eq 2) terminated at different number of terms illustrating no significant improvement in the fit beyond κ_4. (b) Top: simulated scattering from the 3D chain PDF projected down to the flow-gradient plane; bottom: slice-averaged 1D intensity along $q_y = 0$ (Fourier-space equivalent of $\psi_{avg,1D}$ in the flow direction) with the Gram−Charlier fit in q-space (eq 4) indicating the significant increase in the q-range for fitting achieved on including the higher-order $\{\kappa_n\}$ as compared to a Gaussian fit.

degree of scattering anisotropy between different simulation models can be quantitatively assessed using the so-called anisotropy factor, which involves a cosine-weighted expansion of the annularly averaged intensity:

$$A_{f,\cos}(q) = \frac{\int_0^{2\pi} I(q, \phi_s)\cos 2(\phi_s - \phi_{s,0})\mathrm{d}\phi_s}{\int_0^{2\pi} I(q, \phi_s)\mathrm{d}\phi_s} \quad (12)$$

where $\phi_{s,0}$ is the reference angle corresponding to the angle of intensity peaks and $\phi_s = 0$ corresponds to the negative flow axis. The reference angle is chosen to be $\pi/2$ in this case and is perpendicular to the flow direction. Comparing the *Wi*-dependence of A_f across the different polymer simulation models (Figure 6b) shows that the Hookean (Rouse) chain model exhibits the strongest degree of anisotropy at elevated *Wi*, whereas the FENE chain of the bead parameter $b_m = 450$ exhibits the weakest degree of anisotropy, as expected as these models correspond to the most and least extensible chains and consistent with the results for the real-space PDFs (Figure 3).

While A_f allows one to quantify the relative anisotropy exhibited by the different models, it is only a scalar parametrization of the intensity and is not immediately interpretable with respect to the detailed polymer chain configuration, thus not giving any direct physical insight into the physics of chain stretch during flow.

Validating a Quasi-1D Gram−Charlier Analysis of Anisotropic Polymer Scattering. Scattering captures details about the complete three-dimensional density distribution within a test material, which becomes anisotropic as the microstructure becomes deformed. However, extracting real-space information regarding the full 3D probability density function (PDF) from a projected 2D scattering pattern poses mathematical challenges.[84] Although projecting a comprehensive 3D G-C analysis onto the 2D scattering (q_x, q_y) plane could be a potential solution, it becomes complex due to the convolution of higher-order moments κ_n across the different directions and is therefore not within the scope of the present study. As a first step of validating the G-C analysis framework, we therefore resort to an approximate, "quasi-1D" analysis of the Gram−Charlier expansion and use it to fit an appropriate one-dimensional average of the anisotropic scattering. We validate this 1D analysis scheme by comparing the higher-order cumulants extracted from the G-C analysis of a 1D-averaged (in r-space) $\psi_{avg}(r)$ to a 1D-averaged (in q-space) predicted $I(q)$. The hypothesis embedded in this analysis is that the non-Gaussian conformational features exhibit a dominant mode along the primary direction of polymer stretching. Agreement between the real-space and Fourier-space non-Gaussian parameters would therefore imply that the non-Gaussian moments of the full 3D PDF are adequately approximated assuming that the entirety of the non-Gaussian behavior is dominated by the components of the cumulants along the stretching direction. If this correspondence can be established, then the analysis can also be used to test the robustness of the G-C method in estimating non-Gaussian conformational features. For example, we examine the effect of terminating the G-C expansion at different κ_n, as well as the ability of the analysis scheme to resolve the different κ_n's upon the addition of experimentally realistic noise. To accomplish these validative studies, it is imperative to use simulated data such that the "true" PDF (obtained through molecular

https://doi.org/10.1021/acs.macromol.4c01169
Macromolecules 2024, 57, 9518−9535

simulations in this instance) is known, offering an absolute measure of error in the analysis.

We first examine the ability of the 1D form of the G-C expansion of the segment density PDF $\psi(x)$ (eq 2) and the corresponding expansion for the scattered intensity $I(q)$ (eq 4) to yield equivalent results for the case where the "true" distribution is known. To do so, the 3D time-averaged segment density PDF obtained from the molecular simulations is integrated over the r_y and r_z directions to obtain a 1D projection of the real-space PDF $\psi_{avg}(r_x)$ (Figure 8a) as in the analysis of Figure 3. This 1D PDF is then fit using a nonlinear regression scheme to the real-space G-C expansion eq 2 to a desired number of terms to obtain best-fit values of the Gaussian width σ and the higher-order non-Gaussian cumulants $\{\kappa_n\}$. We then perform an analogous reduction and fitting in Fourier space, whereby eq 11 is first used to compute the 3D scattering intensity $I(q_x, q_y, q_z = 0)$ predicted from the full 3D PDF (where we have assumed that $I_0 = 1$ for simplicity, as this does not alter the q-dependence). In the analysis to follow, we perform a slice average of the 2D pattern $I(q_x, q_y, q_z)$ by averaging all the intensities along the x-direction for a slice about $q_y = 0$ thereby producing a 1D-averaged intensity $I_{avg}(q_x)$ as shown in Figure 8b. Alternatively, one may choose to perform the 1D average along a slice that rotates with the primary axis of anisotropy of the scattering pattern (i.e., the direction of the primary chain orientation). A comparison between these two alternatives (see Section S7) shows that, for the data examined here, the resulting cumulants extracted from the Gram−Charlier analysis are insensitive to choice of direction for 1D averaging—either along the flow direction coincident with q_x or the direction of primary orientation.

We then perform fitting of $I_{avg}(q_x)$ over the entire q-range to the Fourier-space form of the G-C expansion (eq 4) and obtain the resulting best-fit values of σ and $\{\kappa_n\}$. We also perform a Gaussian fit to the same q-range by just using the same expression for the intensity as eqn.4 but without the higher-order cumulants $\{\kappa_n\}$ to highlight the differences in the fits.

In general, we find excellent quantitative agreement in the obtained Gaussian and non-Gaussian cumulants over a range of simulation models and conditions. This is demonstrated by representative data in Figure 7 and the accompanying best-fit G-C parameters (including terms up to κ_8 in Table 1 extracted from simulations of a five-bead Rouse chain at $Wi = 10$). First, we observe that in both the real-space and Fourier-space versions of the analysis, the G-C expansion fit (black lines in Figure 7) provides a much more accurate description of the PDF compared to an equivalent Gaussian fit (red lines in Figure 7), confirming the non-Gaussian nature of the PDF of the deformed polymer chains. Specifically, in the Fourier-space representation, we see excellent agreement of the G-C analysis with the data over the entire computed q-range until $q \sim 0.1$, beyond which scattering probes the intersegmental correlations of the chain which are not adequately described by either the molecular simulations or the G-C analysis. The inset plot in Figure 7b shows that in the low-q limit, the assumption of the Gaussian conformational distribution is valid and both fits do a good job, but the Gaussian fit becomes progressively worse as you increase the q-range for fitting. Thus, with the Gram−Charlier expansion, we significantly broadens the q-range that can be described for a nonlinearly deformed chain compared to the Guinier−Rouse analysis which has been described in detail in Section S3. More importantly, we find that the cumulants extracted from fitting the real-space PDF to eq 2 are identical to the cumulants extracted from fitting eq 4 to the q-space scattering intensity. This validates the 1D form of the G-C analysis and demonstrates that a simple analytical G-C analysis of anisotropic polymer scattering (in this case, appropriately averaged to a 1D spectrum) can be used to characterize both the overall chain dimension (represented by σ) and its non-Gaussian characteristics (represented by $\{\kappa_n\}$) simultaneously.

Table 1. Fit Parameters in Real and Fourier Space for a Five-Bead Hookean Chain at $Wi = 10$

Fit parameters	Real space	Fourier space
$[\kappa_4/(4!\sigma^4)] \times 10^3$	6.28 ± 0.14	6.24 ± 0.13
$[\kappa_6/(6!\sigma^6)] \times 10^5$	−10.2 ± 1.21	−10.2 ± 1.12
$[\kappa_8/(8!\sigma^8)] \times 10^7$	86.24 ± 8.32	86.11 ± 7.71

Having established the interchangability of the real- and Fourier-space forms of the G-C analysis and its accuracy in describing non-Guassian features of the polymer PDF, we then examined the sensitivity of the analysis to closing the G-C expansion at increasingly higher-order cumulants. This both tests for convergence of the expansion and informs future determinations of how many cumulants are needed to describe various forms of non-Gaussian conformations. The results, shown for the five-bead Rouse model at $Wi = 10$ in Figure 7a with corresponding parameter values in Table 2, show that the G-C fit to any number of cumulants possesses better agreement with the simulated real-space PDF compared to an equivalent Gaussian fit, especially at the tails of the distribution where the Gaussian fit under predicts. It will be pointed out later that these "long tails" of the distribution contribute the most to the nonlinear physics of the chain deformation. Nevertheless, we find that the G-C expansion fits at different levels of truncation of the higher-order cumulants do not appreciably improve beyond the first correction to the Gaussian κ_4. Furthermore, the data in Table 2 demonstrate that the particular best-fit values of a particular $\{\kappa_n\}$ are insensitive to the number of terms retained in the expansion. This confirms that the G-C expansion is convergent even for a small number of non-Gaussian corrections and provides confidence that the overall shape of the non-Gaussian PDF extracted from scattering data is insensitive to the number of terms retained, even when considerable non-Gaussian behavior is observed.

In real experimental scattering measurements, the measured scattering intensities are convoluted with statistical sampling noise and detector noise. While it is difficult to simulate statistical noise that arises due to sampling errors, it is easier to simulate the random detector noise, which manifests as signal-to-noise ratios in experimental scattering data. To evaluate the effects of such noise on the accuracy and precision of the G-C analysis, we added Gaussian noise of varying relative error levels (refer to Figure S8) to the predicted intensity. We observe that for noise levels less than ∼4% of the simulated scattering intensity, the values of κ_4, κ_6, and κ_8 can be estimated precisely; that is, the best-fit values remain insensitive to the level noise, and their value is statistically distinguishable from zero. For noise levels above 4%, confidence intervals in the best-fit values of κ_6 and κ_8 exceed half the magnitude of the

https://doi.org/10.1021/acs.macromol.4c01169
Macromolecules 2024, 57, 9518−9535

Table 2. Fit Parameters from the Expansion Scheme at Various Levels of Series Truncation for a Five-Bead Hookean Chain at $Wi = 10$

Fit parameters	Gaussian fit	G-C fit: 2 terms	G-C fit: 3 terms	G-C fit: 4 terms
σ	3.53 ± 0.03	3.53 ± 0.03	3.53 ± 0.03	3.53 ± 0.03
$[\kappa_4/(4!\sigma^4)] \times 10^3$		6.28 ± 0.16	6.45 ± 0.15	6.24 ± 0.14
$[\kappa_6/(6!\sigma^6)] \times 10^5$			−7.94 ± 1.34	−10.2 ± 1.21
$[\kappa_8/(8!\sigma^8)] \times 10^7$				86.1 ± 8.32

best-fit value, and as such, these higher-order cumulants cannot be properly resolved above this level of noise. However, we note that the level of noise in general has no other noticeable compromising effect on the magnitude of the best-fit values. As such, we find that the G-C analysis is robust to experimentally realistic levels of noise in the scattering intensity, though caution should be taken when attempting to interpret the highest-order cumulants when the noise level exceeds this threshold. Because of this, and because the qualitative shape of the PDF extracted from the cumulants is insensitive to κ_6 and κ_8 in this particular study, we primarily restrict the comparative analysis of non-Gaussian behavior of different simulation models to follow the interpretation of κ_4 only.

Comparative Analysis of Non-Gaussian Behavior among Polymer Simulation Models Using the G-C Analysis. Having established the validity of the G-C analysis for extracting features of non-Gaussian deformed polymer conformations, we now use the simulated data to demonstrate a useful application of the analysis—to compare the non-Gaussian features of different mechanical models of nonlinear polymer elasticity and in so doing identify distinguishing features of these models. In principle, doing so on experimentally measured data could then be used to propose accurate models (or, in the best case, model parameters) directly from the data without the need for detailed molecular simulations.

We explore this idea by applying the G-C analysis as just described to the simulated data sets involving both Rouse and FENE-type models of chain extensibility, in both the absence and presence of hydrodynamic interactions. In general, we find that the G-C analysis reveals noticeable distinctions in the extracted non-Gaussian parameters among the different polymer models. For example, Figure 8 compares the results obtained for a Rouse chain (with Hookean elastic forces between beads) and a finitely extensible chain (with FENE-type elastic forces given by eq 7). As a comparative measure of overall polymer stretch relative to the equilibrium configuration (at $Wi = 0$), we compute $\frac{\sigma(Wi)}{\sigma(Wi=0)}$ and examine $\frac{\kappa_4(Wi)}{4!\,(\sigma(Wi))^4}$—which is the prefactor on the first non-Gaussian correction term in eq 4 and is therefore a measure of the overall degree of non-Gaussian deformation of the segment density PDF.

We first assess the resulting differences in the overall degree of polymer stretch $\frac{\sigma(Wi)}{\sigma(Wi=0)}$ (Figure 8a). We expect that the degree of stretching for polymer chains at equivalent Wi values should be proportional to the degree of overall chain extensibility. This is consistent with the results observed in Figure 8a, where $\sigma_{Wi}/\sigma_{Wi=0}$ increases the most over the range of Wi for the Rouse chain and the least for the FENE chain with the lowest degree of extensibility ($b_m = 450$). For the case of the Rouse chain, the results can be understood analytically

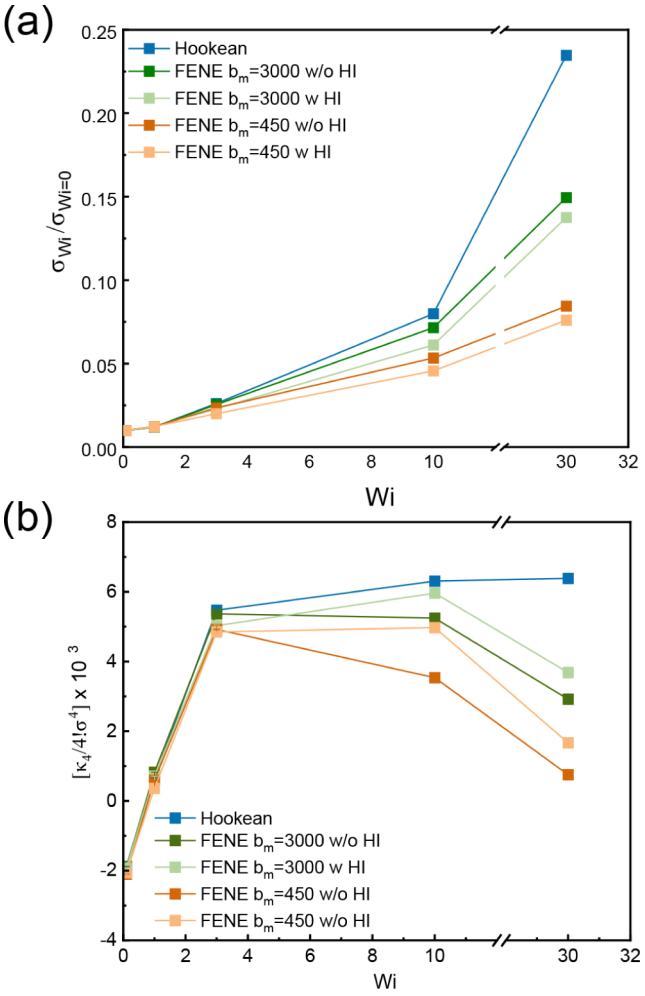

Figure 8. Results of G-C analysis applied to simulations of an isolated $N = 5$ bead polymer in shear flow at various Wi. (a) Increase in the average Gaussian width (σ) relative to equilibrium ($Wi = 0$) of the segment density distribution ψ_{avg} with increasing Wi indicating chain stretch in flow. (b) Changes in the normalized fourth cumulant κ_4 with increasing Wi showing clear differences between Rouse and FENE chains. Error bars representing the confidence intervals associated with the best-fit values are smaller than the data points. Lines are drawn to guide the eye.

by examining the behavior of the components of the gyration tensor $\boldsymbol{G}$ (eqn. S16); specifically, G_{xx} is expected to grow as $\sim Wi^2$. In the case of the FENE-type models, we generally find that the degree of stretch at fixed Wi is more sensitive to the extensibility parameter b_m than on the presence or absence of hydrodynamic interactions (HI) in the simulations, although the presence of HI tends to suppress the stretching of the polymer chain for all Wi. Importantly, we note that although the influence of finite extensibility leads to significant

https://doi.org/10.1021/acs.macromol.4c01169
Macromolecules 2024, 57, 9518−9535

quantitative differences in the *Wi*-dependence of the overall polymer stretch, the behavior is qualitatively similar for all models examined. In particular, if one were to examine one of the curves in Figure 8a in isolation (as would be the case in an experiment), it would be difficult to identify *a priori* whether the data belong to the Rouse model or the FENE model.

By contrast, the non-Gaussian characteristics of the simulated deformed polymers exhibit qualitatively different *Wi*-dependence, depending on the simulation model used for the segmental extensibility. First, we describe the behavior of κ_4 with increasing *Wi* for the Rouse chain (Figure 8b, blue points). Even at $Wi = 0$, we see a nonzero κ_4 because the average PDF for a Rouse chain is a sum of different Gaussian PDFs which contrary to our intuition is not a Gaussian distribution. For nonzero *Wi*, κ_4/σ^4 increases with increasing *Wi*, indicating an increasing degree of non-Gaussian shape in the segment density PDF. As shown previously in Figures 3 and 4, this increasing non-Gaussian character arises due to an increasing disparity in the amount of (Gaussian) stretching of the different individual bead pairs along the chain contour. However, for sufficiently large *Wi* ($Wi \sim 10$), κ_4/σ^4 saturates to a value that is insensitive to further increases in *Wi*, indicating that the segment PDF achieves a self-similar shape, whose non-Gaussian characteristics are insensitive to the amount of stretch on the chain even as σ continues to increase. This behavior can be understood by considering a normal-mode analysis of the Rouse chain (refer to Section S3), in which the longest relaxation time λ_1 (on which *Wi* is scaled) represents the dynamics associated with stretching of the longest chain distance and shorter relaxation times ($\{\lambda_i\}$) represent the dynamics associated with shorter subchains. Because of this spectrum of relaxation modes, when $Wi > 1$, this produces a cascade of subchain stretching that proceeds to stretch increasingly higher normal modes (i.e., smaller subchain segments). Initially, for sufficiently small *Wi*, only the longest modes will become stretched, while the shortest modes retain their equilibrium distribution, and this will exacerbate the effects seen in Figure 4, whereby a "long tail" of the segment density PDF emerges due to the inhomogeneity of stretch on individual bead pairs, resulting in an increasingly positive value of κ_4/σ^4. However, for sufficiently large *Wi*, all of the normal modes will become strongly stretched such that the *Wi*-dependent contributions dominate the normal modes (cf., eq S11), and it is at this point we expect that the segment PDF will achieve a self-similar shape and therefore a value of κ_4/σ^4 that is independent of *Wi*.

A very different scenario is observed for the *Wi*-dependence of non-Gaussian behavior for simulations of FENE-type chains (Figure 8b, green and orange points), in which κ_4/σ^4 first increases with *Wi* until $Wi \sim 3$, only to then decrease with increasing *Wi* even as the chain becomes more stretched (i.e., σ continues to increase). Because κ_4/σ^4 measures the overall degree of deformation of the polymer chain segment PDF away from a reference Gaussian distribution, this result would naïvely suggest that non-Gaussian character first increases and then deacreases as *Wi* is increased, indicating a return to near-Gaussian behavior at sufficiently large *Wi*. Instead, we argue that the nonmonotonic changes in κ_4/σ^4 with increasing *Wi* occur due to a competition between two competing effects—one that makes a positive contribution to κ_4 and another that makes a negative contribution to κ_4. The first effect is the same one just described for the Rouse model—for moderate *Wi*, changes in the relative stretch experienced across the different normal modes act to increase the value κ_4/σ^4 with increasing *Wi*. We observe that this effect is preserved even for a chain of FENE-type springs—this is evident in the PDFs of individual bead pairs for the FENE model when $Wi = 1$ (Figure S5), which are qualitatively similar to those obtained for the Rouse model under equivalent conditions. However, a second effect arises due to the limited extensibility of the individual bead pairs. As discussed previously, as the individual bead−spring pairs become sufficiently stretched so that their finite extensibility is approached, which leads to flattening in the center of the individual bead pair PDF (Figure 5) for pairs closest to the middle of the chain as these segments experience the largest degree of stretching. The dominant effect of this behavior on the average segment density PDF for the entire chain is to flatten the central peak of the distribution relative to an equivalent Rouse chain, and this flattening makes a net negative contribution to κ_4/σ^4 that increases with increasing *Wi*. For sufficiently large *Wi*, the effect of this negative contribution to κ_4/σ^4 overcomes the positive contribution coming from the spectrum of normal modes, leading to the observed maximum and then decrease in κ_4/σ^4 for $Wi > 3$. We observe that this behavior is exacerbated as the chains become less extensible, that is, as the value of b_m decreases, such that κ_4/σ^4 decreases more sharply with increasing *Wi* after the maximum, consistent with the above explanation. Interestingly, we also note that the influence of HI on κ_4/σ^4 becomes significantly more pronounced after the maximum, suggesting that the importance of HI on the non-Gaussian features of the chain configuration is strongly coupled to the effects of nonlinear elasticity and finite extensibility for the case of FENE-type models.

In summary, we find that nonlinear deformations of idealized polymer chains in shear flow are accompanied by significant non-Gaussian features in their segment density PDF and that these features produce quite different qualitative behavior in the cumulants of the PDF accessible by the G-C analysis depending on the molecular model adopted to describe the nonlinear chain elasticity. For the case of a Rouse chain, κ_4/σ^4 increases monotonically with increasing *Wi* and achieves a plateau at large *Wi* due to a self-similar evolution of the chain normal modes in this limit. By contrast, for FENE-type chains, flattening of the individual segment PDFs due to finite extensibility with increasing *Wi* produces a net negative contribution to κ_4/σ^4 that ultimately drives nonmonotonic behavior with increasing *Wi*, and this behavior is exacerbated with decreasing chain extensibility and in the presence of hydrodynamic interactions. Importantly, none of these distinguishing features are evident when only the Gaussian width σ of the segment density PDF is examined, emphasizing the need to examine and describe non-Gaussian conformations to understand the physics of nonlinear chain deformation. Moreover, because the G-C analysis of scattering provides detailed access to these non-Gaussian features, the results provide a blueprint for using scattering experiments in flow to give direct and unequivocal insights into the distinct underlying mechanisms governing the nonlinear chain deformation of polymers without having *a priori* knowledge of a specific molecular model to describe the scattering. For

https://doi.org/10.1021/acs.macromol.4c01169
Macromolecules 2024, 57, 9518−9535

example, one could thus use scattering to estimate κ_4/σ^4 using the G-C analysis, and the results could be used to infer whether finite extensibility effects are important for describing the polymer rheology.

CONCLUSION AND OUTLOOK

Very few polymers adopt idealized Gaussian configuration distributions, even though they are frequently assumed when experimental measurements are connected to molecular theories. In this work, we developed a general mathematical framework—based on the concept of moments—to describe and characterize the non-Gaussian features of polymer configurations, both at equilibrium and under applied deformations. Due to its mathematical behavior, the well-established Gram−Charlier expansion method provides an efficient analysis to equivalently extract cumulants of non-Gaussian polymer segment density PDFs from either a real-space distribution (e.g., measured from molecular simulations) or a Fourier-space density spectrum (e.g., measured from small-angle scattering). The resulting cumulants provide a means to "fingerprint" the non-Gaussian conformational landscape of complex and highly deformed polymers that is agnostic to any specific details of the polymer chemistry, topology, or molecular-scale model of the polymer physics.

We validated the G-C analysis of polymer scattering and demonstrated its utility using two case studies—sequence-defined associative heteropolymers (polypeptoids) at equilibrium and computationally simulated homopolymers undergoing nonlinear deformation in shear flow. Using these validative studies, we verified the convergence of the Gram−Charlier series and its robustness with respect to experimentally realizable measurement uncertainty, demonstrating its ability to extract statistically meaningful and physically interpretable non-Gaussian parameters of the configuration distribution. In the case of peptoids, we showed that the introduction of patterned intramolecular associations produces conformations with variable non-Gaussian character depending on their location along the polymer chain, which can be successfully described using higher-order cumulants estimated from experiments using the G-C analysis. In the case of deformed polymers in flow, we applied the G-C analysis to emulate scattering from molecular simulations involving various common molecular models of polymer mechanics and rheology. The results showed that even ideal Rouse-like polymers exhibit "long-tailed" non-Gaussian segment density PDFs due to their distribution of normal modes. While nonlinear deformations enhance this dispersity, finite extensibility produces flat-peaked non-Gaussian distributions, and these two competing effects produce distinct features in the higher-order non-Gaussian cumulants that can be estimated from scattering data. We therefore propose that the G-C analysis can be used to distinguish different molecular polymer models from data with no *a priori* knowledge of which particular model a test polymer is best described by.

Overall, we find that the G-C analysis of polymer scattering holds potential for generally characterizing the non-Gaussian behavior of complex polymers both at and out of equilibrium. We envision that G-C analysis will become useful for a number of different applications of contemporary interest in polymer research, including heteropolymers, topology-defined polymers, and polymers experiencing complex or nonlinear deformations. We anticipate that these applications will motivate further refinements and interpretations of the G-C analysis scheme that we have proposed here. For example, the present work was limited to a 1D version of the G-C expansion, and we found that a 1D analysis is largely sufficient to describe the non-Gaussian features of polymer scattering even when the polymer configuration is anisotropic, as long as care is taken to perform an appropriate 1D average of the scattering data. However, a 1D analysis will likely prove insufficient for cases where the 3D configuration is sufficiently complex such as for polymers experiencing complex or time-varying deformation fields. Such cases will likely require extension of the G-C analysis to 2*D*/3D, and such efforts are the subject of ongoing work.

In conclusion, the G-C analysis presented here provides an efficient and compact method to mathematically describe non-Gaussian characteristics of polymer conformations. By extracting the series of cumulants of the polymer segment PDF, one can use G-C analysis of polymer scattering to directly visualize and physically interpret non-Gaussian configurations and the processes that give rise to them. We hope that this work will inspire researchers to further investigate the importance of non-Gaussian characteristics in describing and predicting polymer structure, dynamics, and properties.

ASSOCIATED CONTENT

Supporting Information

The Supporting Information is available free of charge at https://pubs.acs.org/doi/10.1021/acs.macromol.4c01169.

Details regarding Gram−Charlier expansion; DEER characterization for the peptoids and details of the GC-expansion and excluded volume fit parameters; normal-mode analysis for Rouse chains in shear flow; Guinier−Rouse model to predict scattering from Rouse chains in shear flows in the low-q limit; details of Brownian dynamics simulations; effect of chain discretization on the average segment density distribution; one-dimensional averaging directions to apply 1D−Gram Charlier analysis to scattering intensities; sensitivity of fit parameters to noise (PDF)

AUTHOR INFORMATION

Corresponding Authors

Patrick T. Underhill − *Department of Chemical and Biological Engineering, Rensselaer Polytechnic Institute, Troy, New York 12180, United States;* orcid.org/0000-0002-0329-8370; Email: underp3@rpi.edu

Matthew E. Helgeson − *Department of Chemical Engineering, University of California Santa Barbara, Santa Barbara, California 93106-5080, United States;* orcid.org/0000-0001-9384-4023; Email: helgeson@ucsb.edu

Authors

Anukta Datta − *Department of Chemical Engineering, University of California Santa Barbara, Santa Barbara, California 93106-5080, United States*

Xiaoyan Wang − *Department of Chemical and Biological Engineering, Rensselaer Polytechnic Institute, Troy, New York 12180, United States*

Shawn D. Mengel − *Department of Chemical Engineering, University of California Santa Barbara, Santa Barbara,*

California 93106-5080, United States; orcid.org/0000-0003-3821-818X

Audra J. DeStefano − *Department of Chemical Engineering, University of California Santa Barbara, Santa Barbara, California 93106-5080, United States;* orcid.org/0000-0003-1047-2637

Rachel A. Segalman − *Department of Chemical Engineering, University of California Santa Barbara, Santa Barbara, California 93106-5080, United States;* orcid.org/0000-0002-4292-5103

Complete contact information is available at: https://pubs.acs.org/10.1021/acs.macromol.4c01169

Notes

The authors declare no competing financial interest.

■ ACKNOWLEDGMENTS

This work was primarily funded by the U.S. Department of Energy, Office of Science, Basic Energy Science under award numbers DE-SC0020988 and DE-SC0021294. Polypeptoid synthesis and characterization were supported by the National Science Foundation under grant no. 2203179 (S.D.M., A.J.D., and R.A.S.) leveraging facilities and expertise from the BioPACIFIC Materials Innovation Platform of the National Science Foundation under award no. DMR-1933487. S.D.M. acknowledges support from the National Science Foundation Graduate Research Fellowship (DGE 2139319). A.J.D. acknowledges support from the Department of Defense through the National Defense Science & Engineering Graduate (NDSEG) Fellowship Program. A portion of this research used resources at the Spallation Neutron Source, as appropriate, a DOE Office of Science User Facility operated by the Oak Ridge National Laboratory.

■ REFERENCES

(1) Doi, M.; Edwards, S. F.; Edwards, S. F. *The Theory of Polymer Dynamics*; Oxford University Press, 1988; Vol. *73*.

(2) Rubinsten, M. *Polymer physics*; Oxford University Press: United States of America, 2003.

(3) Nagai, K. Non-gaussian character of real polymer chains. *J. Chem. Phys.* **1963**, *38*, 924−933.

(4) Saito, N.; Takahashi, K.; Yunoki, Y. The statistical mechanical theory of stiff chains. *J. Phys. Soc. Jpn.* **1967**, *22*, 219−226.

(5) Goto, S.; Kim, K.; Matubayasi, N. Effects of chain length on Rouse modes and non-Gaussianity in linear and ring polymer melts. *J. Chem. Phys.* **2021**, *155* (12), 124901.

(6) Smith, G. D.; Paul, W.; Monkenbusch, M.; Richter, D. On the non-Gaussianity of chain motion in unentangled polymer melts. *J. Chem. Phys.* **2001**, *114*, 4285−4288.

(7) Kruteva, M.; Zamponi, M.; Hoffmann, I.; Allgaier, J.; Monkenbusch, M.; Richter, D. Non-Gaussian and Cooperative Dynamics of Entanglement Strands in Polymer Melts. *Macromolecules* **2021**, *54*, 11384−11391.

(8) Chen, J. Z. Theory of wormlike polymer chains in confinement. *Prog. Polym. Sci.* **2016**, *54*−*55*, 3−46.

(9) Richter, D.; Kruteva, M. Polymer dynamics under confinement. *Soft Matter* **2019**, *15*, 7316−7349.

(10) Michieletto, D.; Nahali, N.; Rosa, A. *Glassiness and Heterogeneous Dynamics in Dense Solutions of Ring Polymers*; American Physical Society, 2017.

(11) Gerashchenko, S.; Steinberg, V. Statistics of tumbling of a single polymer molecule in shear flow. *Phys. Rev. Lett.* **2006**, *96*, 038304.

(12) Fixman, M.; Kovac, J. Polymer conformational statistics. III. Modified Gaussian models of stiff chains. *J. Chem. Phys.* **1973**, *58*, 1564−1568.

(13) Fixman, M.; Skolnick, J. Moments and distribution function of polymer chains. *J. Chem. Phys.* **1976**, *65*, 1700−1707.

(14) Yamakawa, H. Stiff-Chain Macromolecules. *Annu. Rev. Phys. Chem.* **1984**, *35*, 23−47.

(15) Knudsen, K. D.; Torre, J. G.; Elgsaeter, A. Gaussian chains with excluded volume and hydrodynamic interaction: Shear rate, dependence of radius of gyration, intrinsic viscosity and flow birefringence. *Polymer* **1996**, *37*, 1317−1322.

(16) Pierleoni, C.; Ryckaert, J.-P. Excluded Volume Effects on the Structure of a Linear Polymer under Shear Flow. *J. Chem. Phys.* **2000**, *113*, 5545−5558.

(17) Li, Y.; Yao, P.; Guo, H. Non-Rouse behavior of short ring polymers in melts by molecular dynamics simulations. *Soft Matter* **2023**, *19*, 7161−7171.

(18) Rosales, A. M.; Murnen, H. K.; Kline, S. R.; Zuckermann, R. N.; Segalman, R. A. Determination of the persistence length of helical and non-helical polypeptoids in solution. *Soft Matter* **2012**, *8*, 3673−3680.

(19) Hur, J. S.; Shaqfeh, E. S. G.; Larson, R. G. Brownian dynamics simulations of single DNA molecules in shear flow. *J. Rheol.* **2000**, *44*, 713−742.

(20) Larson, R. G. The rheology of dilute solutions of flexible polymers: Progress and problems. *J. Rheol.* **2005**, *49*, 1−70.

(21) De Gennes, P. G. Coil-stretch transition of dilute flexible polymers under ultrahigh velocity gradients Coil-stretch transition of dilute flexible polymers under ultrahigh velocity gradients. *J. Chem. Phys.* **1974**, *60*, 5030−5042.

(22) Larson, R. G.; Magda, J. J. Coil-Stretch Transitions in Mixed Shear and Extensional Flows of Dilute Polymer Solutions. *Macromolecules* **1989**, *22* (7), 3004−3010.

(23) Doyle, P. S.; Shaqfeh, E. S. G. Dynamic simulation of freely-draining, flexible bead-rod chains: Start-up of extensional and shear flow. *J. Non-Newtonian Fluid Mech.* **1998**, *76*, 43−78.

(24) Smith, D. E.; Babcock, H. P.; Chu, S. Single-polymer dynamics in steady shear flow. *Science* **1999**, *283*, 1724−1727.

(25) Bird, R.; Curtiss, C.; Armstrong, R.; Hassager, O. *Dynamics of Polymeric Liquids, Vol. 2: Kinetic Theory*, 2nd ed.; Wiley, 1987.

(26) Jarecki, L.; Misztal-Faraj, B. Non-linear stress-orientation behavior of flexible chain polymers under fast elongational flow. *Eur. Polym. J.* **2017**, *95*, 368−381.

(27) Benoit, H.; Decker, D.; Higgins, J. S.; Picot, C.; Cotton, J. P.; Farnoux, B.; Jannink, G.; Ober, R. Dimensions of a Flexible Polymer Chain in the Bulk and in Solution. *Nat. Phys. Sci.* **1973**, *245*, 13−15.

(28) Yamakawa, H. *Modern theory of polymer solutions*; Harper & Row, 1971.

(29) Isihara, A. Probable Distribution of Segments of a Polymer Around the Center of Gravity. *J. Phys. Soc. Jpn.* **1950**, *5*, 201A−201A.

(30) Debye, P.; Bueche, F. Distribution of Segments in a Coiling Polymer Molecule. *J. Chem. Phys.* **1952**, *20* (8), 1337−1338.

(31) Wang, Z. G. 50th Anniversary Perspective: Polymer Conformation - A Pedagogical Review. *Macromolecules* **2017**, *50*, 9073−9114.

(32) Fuller, G. G.; Leal, L. G. Flow birefringence of dilute polymer solutions in two-dimensional flows. *Rheol. Acta* **1980**, *19*, 580−600.

(33) Lee, E. C.; Solomon, M. J.; Muller, S. J. Molecular orientation and deformation of polymer solutions under shear: A flow light scattering study. *Macromolecules* **1997**, *30*, 7313−7321.

(34) Russell, T. P. On the reflectivity of polymers: Neutrons and X-rays. *Physica B* **1996**, *221*, 267−283.

(35) Higgins, J.; Benoit, C. *Polymer International*; Oxford University Press, 1994.

(36) Peterlin, A.; Heller, W.; Nakagaki, M. Light Scattering and Statistical Shape of Streaming Freely Flexible Linear Macromolecules. *J. Chem. Phys.* **1958**, *28*, 470−476.

(37) Perkins, T. T.; Smith, D. E.; Larson, R. G.; Chu, S. Stretching of a Single Tethered Polymer in a Uniform Flow. *Science* **1995**, *268*, 83−87.

(38) Smith, D. E.; Chu, S. Response of flexible polymers to a sudden elongational flow. *Science* **1998**, *281*, 1335−1340.

(39) Schroeder, C. M.; Shaqfeh, E. S.; Chu, S. Effect of hydrodynamic interactions on DNA dynamics in extensional flow: Simulation and single molecule experiment. *Macromolecules* **2004**, *37*, 9242−9256.
(40) Shaqfeh, E. S. G. The dynamics of single-molecule DNA in flow. *J. Non-Newtonian Fluid Mech.* **2005**, *130*, 1−28.
(41) Pfannebecker, V.; Klos, H.; Hubrich, M.; Volkmer, T.; Heuer, A.; Wiesner, U.; Spiess, H. W. Determination of end-to-end distances in oligomers by pulsed EPR. *J. Phys. Chem.* **1996**, *100*, 13428−13432.
(42) Sherck, N.; Webber, T.; Brown, D. R.; Keller, T.; Barry, M.; Destefano, A.; Jiao, S.; Segalman, R. A.; Fredrickson, G. H.; Shell, M. S.; Han, S. End-to-End Distance Probability Distributions of Dilute Poly(ethylene oxide) in Aqueous Solution. *J. Am. Chem. Soc.* **2020**, *142*, 19631−19641.
(43) Schuler, B.; Soranno, A.; Hofmann, H.; Nettels, D. Single-Molecule FRET Spectroscopy and the Polymer Physics of Unfolded and Intrinsically Disordered Proteins. *Annu. Rev. Biophys.* **2016**, *45*, 207−231.
(44) Rajdev, P.; Ghosh, S. Fluorescence Resonance Energy Transfer (FRET): A Powerful Tool for Probing Amphiphilic Polymer Aggregates and Supramolecular Polymers. *J. Phys. Chem. B* **2019**, *123*, 327−342.
(45) Schroeder, C. M. Single polymer dynamics for molecular rheology. *J. Rheol.* **2018**, *62*, 371−403.
(46) Menasveta, M. J.; Hoagland, D. A. Light Scattering from Dilute Poly(styrene) Solutions in Uniaxial Elongational Flow. *Macromolecules* **1991**, *24*, 3427−3433.
(47) Zisenis, M.; Springer, J. Rheooptical detection of shear-induced orientation of high molar mass polystyrene in dilute solution. *Polymer* **1994**, *35*, 3156−3163.
(48) Link, A.; Springer, J. Light Scattering from Dilute Polymer Solutions in Shear Flow. *Macromolecules* **1993**, *26*, 464−471.
(49) Lee, E. C.; Muller, S. J. Flow light scattering studies of polymer coil conformation in solutions under shear: Effect of solvent quality. *Polymer* **1999**, *40*, 2501−2510.
(50) Eberle, A. P.; Porcar, L. Flow-SANS and Rheo-SANS applied to soft matter. *Curr. Opin. Colloid Interface Sci.* **2012**, *17*, 33−43.
(51) Hammouda, B. *Probing Nanoscale Structures - The SANS Toolbox*; Center for Neutron Research, 2016.
(52) Debye, P. Molecular weight determination by light scattering. *J. Phys. Coll. Chem.* **1947**, *51*, 18−32.
(53) Rooks, J.; Gilbert, P. H.; Porcar, L.; Liu, Y.; Butler, P. Anisotropy factors in small-angle scattering for dilute rigid-rod suspensions. *J. Appl. Crystallogr.* **2023**, *56*, 683−696.
(54) Wang, Z.; Lam, C. N.; Chen, W. R.; Wang, W.; Liu, J.; Liu, Y.; Porcar, L.; Stanley, C. B.; Zhao, Z.; et al. Fingerprinting molecular relaxation in deformed polymers. *Phys. Rev. X* **2017**, *7*, 031003.
(55) Wang, Z. Y.; Kong, D.; Yang, L.; Ma, H.; Su, F.; Ito, K.; Liu, Y.; Wang, X.; Wang, Z. Analysis of Small-Angle Neutron Scattering Spectra from Deformed Polymers with the Spherical Harmonic Expansion Method and a Network Model. *Macromolecules* **2018**, *51*, 9011−9018.
(56) Huang, G. R.; Wang, Y.; Do, C.; Shinohara, Y.; Egami, T.; Porcar, L.; Liu, Y.; Chen, W. R. Orientational Distribution Function of Aligned Elongated Molecules and Particulates Determined from Their Scattering Signature. *ACS Macro Lett.* **2019**, *8*, 1257−1262.
(57) Huang, G. R.; Wang, Y.; Do, C.; Porcar, L.; Shinohara, Y.; Egami, T.; Chen, W. R. Determining Gyration Tensor of Orienting Macromolecules through Their Scattering Signature. *J. Phys. Chem. Lett.* **2019**, *10*, 3978−3984.
(58) Huang, G. R.; Carrillo, J. M.; Wang, Y.; Do, C.; Porcar, L.; Sumpter, B.; Chen, W. R. An exact inversion method for extracting orientation ordering by small-angle scattering. *Phys. Chem. Chem. Phys.* **2021**, *23*, 4120−4132.
(59) Zhang, J.; Smith, G. S.; Corona, P. T.; Underhill, P. T.; Leal, L. G.; Helgeson, M. E. Self-Consistent Connected-Rod Model for Small-Angle Scattering from Deformed Semiflexible Chains in Flow. *Macromolecules* **2024**, *57*, 201−216.
(60) Yoon, D. Y.; Flory, P. J. Moments and distribution functions for polymer chains of finite length. II. Polymethylene chains. *J. Chem. Phys.* **1974**, *61*, 5366−5380.
(61) Minato, T.; Hatano, A. Distribution Functions of Polymers with and without Interactions. I. The Distribution Function of the Square Distance of the Center of Mass from One Fixed End of a Polymer Chain. *Polym. J.* **1977**, *9*, 239−251.
(62) Doyle, P. S.; Shaqfeh, E. S. G.; Mckinley, G. H.; Spiegelberg, S. H. Relaxation of dilute polymer solutions following extensional flow. *J. Non-Newtonian Fluid Mech.* **1998**, *76*, 79−110.
(63) Montroll, E. W. Markoff Chains and Excluded Volume Effect in Polymer Chains. *J. Chem. Phys.* **1950**, *18*, 734−743.
(64) Carmichael, J. B. Non-gaussian behavior of model short-chain polymers. *J. Appl. Phys.* **1964**, *35*, 3178−3181.
(65) Zimm, B. H. The scattering of light and the radial distribution function of high polymer solutions. *J. Chem. Phys.* **1948**, *16*, 1093−1099.
(66) Flory, P. J.; Bueche, A. M. Theory of light scattering by polymer solutions. *J. Polym. Sci.* **1958**, *27*, 219−229.
(67) Jiao, S.; Destefano, A.; Monroe, J. I.; Barry, M.; Sherck, N.; Casey, T.; Segalman, R. A.; Han, S.; Shell, M. S. Quantifying Polypeptoid Conformational Landscapes through Integrated Experiment and Simulation. *Macromolecules* **2021**, *54*, 5011−5021.
(68) Del Brio, E. B.; Perote, J. Gram-Charlier densities: Maximum likelihood versus the method of moments. *Insur.: Math. Econ.* **2012**, *51*, 531−537.
(69) Lin, W.; Zhang, J. E. The valid regions of Gram−Charlier densities with high-order cumulants. *J. Comput. Appl. Math.* **2022**, *407*, 113945.
(70) Hsu, H. P.; Paul, W.; Binder, K. Understanding the multiple length scales describing the structure of bottle-brush polymers by Monte Carlo simulation methods. *Macromol. Theory Simul.* **2011**, *20*, 510−525.
(71) DeStefano, A. J.; Mengel, S. D.; Bates, M. W.; Jiao, S.; Shell, M. S.; Han, S.; Segalman, R. A. Control over Conformational Landscapes of Polypeptoids by Monomer Sequence Patterning. *Macromolecules* **2024**, *57*, 1469−1477.
(72) Zhao, J. K.; Gao, C. Y.; Liu, D. The extended Q-range small-angle neutron scattering diffractometer at the SNS. *J. Appl. Crystallogr.* **2010**, *43*, 1068−1077.
(73) Heller, W. T.; Cuneo, M.; Debeer-Schmitt, L.; Do, C.; He, L.; Heroux, L.; Littrell, K.; Pingali, S. V.; Qian, S.; Stanley, C.; Urban, V. S.; Wu, B.; Bras, W. The suite of small-angle neutron scattering instruments at Oak Ridge National Laboratory. *J. Appl. Crystallogr.* **2018**, *51*, 242−248.
(74) Arnold, O.; et al. Mantid - Data Analysis and Visualization Package for Neutron Scattering and μSR Experiments. *Nucl. Instrum. Methods Phys. Res., Sect. A* **2014**, *764*, 156−166.
(75) Heller, W. T.; Hetrick, J.; Bilheux, J.; Borreguero Calvo, J. M.; Chen, W.-R.; Debeer-Schmitt, L.; Do, C.; Doucet, M.; Fitzsimmons, M. R.; Godoy, W. F.; et al. drtsans: The data reduction toolkit for small-angle neutron scattering at Oak Ridge National Laboratory. *SSRN Electron. J.* **2022**, *19*, 101101.
(76) Hammouda, B. SANS from homogeneous polymer mixtures: A unified overview. *Adv. Polym. Sci.* **1993**, *106*, 87−133.
(77) Pelliccioni, A.; Angeloni, M. A new formulation of the Gram-Charlier method: Performance for fitting non-normal distribution. *Nuovo Cimento Soc. Ital. Fis., C* **2007**, *30*, 381−394.
(78) Sørensen, H. O.; Stewart, R. F.; McIntyre, G. J.; Larsen, S. Simultaneous variation of multipole parameters and Gram−Charlier coefficients in a charge-density study of tetrafluoroterephthalonitrile based on X-ray and neutron data. *Acta Crystallogr., Sect. A: Found. Adv.* **2003**, *59*, 540−550.
(79) Doyle, P. S.; Underhill, P. T. *Handbook of Materials Modeling*; Springer: Dordrecht, 2005; pp. 26192630.
(80) Radhakrishnan, R.; Underhill, P. T. Models of flexible polymers in good solvents: Relaxation and coil-stretch transition. *Soft Matter* **2012**, *8*, 6991−7003.

https://doi.org/10.1021/acs.macromol.4c01169
Macromolecules 2024, 57, 9518−9535

(81) Ferry, J. D. *Viscoelastic properties of polymers*; John Wiley & Sons, 1980.
(82) Warner, H. R. Kinetic Theory and Rheology of Dilute Suspensions of Finitely Extendible Dumbbells. *Ind. Eng, Chem. Fundamen.* **1972**, *11*, 379−387.
(83) Winter, H. H. The occurrence of self-similar relaxation in polymers. *J. Non-Cryst. Solids* **1994**, *172-174*, 1158−1167.
(84) Corona, P. T.; Silmore, K. S.; Adkins, R.; Lang, C.; Lettinga, M. P.; Swan, J. W.; Leal, L. G.; Helgeson, M. E. Bayesian estimations of orientation distribution functions from small-angle scattering enable direct prediction of mechanical stress in anisotropic materials. *Phys. Rev. Mater.* **2021**, *5*, 065601−065601.

https://doi.org/10.1021/acs.macromol.4c01169
Macromolecules 2024, 57, 9518−9535